January 2020

Modeling of Gas-Solid Flows in Industry with Computational Fluid Dynamics Tools: An Assessment of Modeling Methodologies and Computational Challenges

Kaylee Smith

MODELING OF GAS-SOLID FLOWS IN INDUSTRY WITH COMPUTATIONAL FLUID DYNAMICS TOOLS: AN ASSESSMENT OF MODELING METHODOLOGIES AND COMPUTATIONAL CHALLENGES

by

KayLee Michelle Smith
Bachelor of Science, University of North Dakota, 2019

A Thesis

Submitted to the Graduate Faculty

of the

University of North Dakota

In partial fulfillment of the requirements

for the degree of

Master of Science

Grand Forks, North Dakota
August
2020

Name: KayLee Smith

Degree: Master of Science

This document, submitted in partial fulfillment of the requirements for the degree from the University of North Dakota, has been read by the Faculty Advisory Committee under whom the work has been done and is hereby approved.

DocuSigned by:
Dr. Gautham Krishnamoorthy
8F9DB14ED5F042D...
Dr. Gautham Krishnamoorthy

DocuSigned by:
Wayne Seames
7064B4041A044CD...
Dr. Wayne Seames

DocuSigned by:
Frank Bowman
543F510845EF4AE...
Dr. Frank Bowman

This document is being submitted by the appointed advisory committee as having met all the requirements of the School of Graduate Studies at the University of North Dakota and is hereby approved.

DocuSigned by:
Chris Nelson
2E0AF088C733403...
Chris Nelson
Dean of the School of Graduate Studies

6/11/2020
Date

PERMISSION

Title: Modeling of Gas-Solid Flows in Industry with Computational Fluid Dynamics Tools: An Assessment of Modeling Methodologies and Computational Challenges

Department: Chemical Engineering

Degree: Master of Science

In presenting this thesis in partial fulfillment of the requirements for a graduate degree from the University of North Dakota, I agree that the library of this University shall make it freely available for inspection. I further agree that permission for extensive copying for scholarly purposes may be granted by the professor who supervised my thesis work or, in his absence, by the Chairperson of the department or the dean of the School of Graduate Studies. It is understood that any copying or publication or other use of this thesis or part thereof for financial gain shall not be allowed without my written permission. It is also understood that due recognition shall be given to me and to the University of North Dakota in any scholarly use which may be made of any material in my thesis.

KayLee Smith

June 9th, 2020

TABLE OF CONTENTS

LIST OF FIGURES

LIST OF TABLES

NOMENCLATURE

A	Pre-exponential factor (in 1/s or kg/m^{2}sPa)
A_c	cross sectional area of OFC reactor (in m^2)
a_{1-3}	coefficients for Morsi-Alexander drag law
a, b	tuning parameter in Syamlal-O'Brien drag law
C_p	specific heat capacity (in kg m^2/s^2 K)
C_D	drag coefficient
d	diameter (in m or cm)
Ea	Activation energy (J/kmol)
$\boldsymbol{F}_T$	total force vector (in N)
$\boldsymbol{F_D}$	drag force vector (in N)
$\boldsymbol{F_C}$	contact force vector (in N)
$\dot{f}$	mass flowrate of fuel (in kg/s)
$\boldsymbol{g}$	gravitational force vector (m/s^2)
H	rate of enthalpy transfer
ΔH_r	heat of reaction

H_{wall}	rate of heat transfer at walls
I_{gm}	rate of interphase momentum transfer
$\bar{\bar{I}}$	identity tensor
m	mass (in kg)
P	pressure (in kPa)
$\boldsymbol{q}$	heat flux vector
q	mass flux
R	rate of interphase mass/species transfer
Re	Reynolds number (dimensionless)
$r_{deposition}$	rate of ash deposition (in kg/m^{2}s)
$\bar{\bar{S}}$	stress tensor
T	temperature (in K)
t	time (in s)
$\boldsymbol{v}$	velocity vector (in m/s)
v	velocity magnitude (in m/s)
w_{ash}	weight fraction of ash

We	Weber number (dimensionless)
$\boldsymbol{X}$	positional vector (Lagrangian frame)
x_i or X_n	mass fraction

Greek Symbols

α_q	void fraction of an arbitrary phase
β	interphase momentum exchange coefficient
ε	void fraction
η	efficiency
η_i	impaction efficiency
η_i	capture efficiency
η_o	overall collection efficiency
σ	surface tension (in N/m)
$\overline{\sigma_\iota}$	partial surface tension coefficient
ρ	density (in kg/m^3)
μ	viscosity (kg/ms)
$\bar{\bar{\tau}}$	stress-strain tensor

∇	gradient
$\boldsymbol{\omega}$	angular velocity vector (m/s)

Subscripts

i	single particle
m	solids phase
g	fluid/gas phase
q or k	arbitrary continuous phase

Important Acronyms

CFD	Computational Fluid Dynamics
MFiX	Multiphase Flow with Interphase Exchanges
PETSc	Portable, Extensible Toolkit for Scientific Computation
DEM	Discrete Element Model (in MFiX)
MPIC	Multiphase Particle in Cell Model (in MFiX)
TFM	Two Fluid Model (in MFiX)
DPM	Discrete Phase Model (in ANSYS Fluent)
NETL	National Energy Technology Laboratory

SSCPI	Small Scale Challenge Problem I
PSD	Particle Size Distribution
PRB	Powder River Basin coal type
RR	Rosin-Rammler
SST	Shear Stress Transport (turbulence model)

ACKNOWLEDGEMETNS

I would first like to extend a heartfelt thank you to my kind, smart, funny, popcorn snacking, and chicken chasing research advisor/mentor/professor, Dr. Gautham Krishnamoorthy. He was the first to encourage me to explore the world of research during my junior year of undergrad by providing me with the opportunity to indulge in my curiosities and take on various small research tasks which challenged me to learn MFiX and ANSYS Fluent simultaneously. I would also like to thank Dr. Krishnamoorthy for leading me to the Mickey Leland Energy Fellowship program through the DOE. I will be forever grateful for the AMAZING experience I had in Morgantown, WV working on a cyber-physical hybrid power system research project at NETL and making professional and personal connections with people from all across the world. Even though I have ~currently~ decided not to go onto a PhD program, which I know probably broke Dr. Krishnamoorthy's heart a little bit, he still continued to help me look for opportunities where my passions and skills would shine best. I will carry the lessons I learned from Dr. Krishnamoorthy about creative technical writing and problem solving through the rest of my engineering career.

Next, I would like to thank my committee members Dr. Frank Bowman and Dr. Wayne Seames for sharing their expertise while finalizing my thesis, and also for their mentorship as professors throughout undergrad. Dr. Bowman was the perfect faculty advisor to work with during my time as President of UND's local chapter of AIChE because he gave

me the free reign and confidence to bring new pep into the organization's step, and was always still there to remind me when something actually important was due. Dr. Seames has never once let me coast through anything, to which in hindsight I am incredibly appreciative of, and he has always been there to push and challenge me to step up into dimensions of leadership and academic rigor that I had never thought I was capable of before.

I would also like to thank all of my family for the sacrifices and efforts they made to help me feel incredibly loved and supported throughout my entire college adventures. They have always been there to help me make it home for the holidays in any way possible and some even came all the way to North Dakota in the dead of winter once for a hockey game on my birthday. I especially want to acknowledge my mom because there are no words to describe how much I love her. She has always been my biggest cheerleader and I couldn't imagine having got to this point in my life without all her love and guidance. I also want to thank my brother for being the funny sibling so that I could be the smart one. Naturally, I also have to acknowledge the one person that helped me both cry and laugh my way through nine semesters of chemical engineering school, so here you go Kalea I appreciate you.

Finally, I would like to acknowledge that this research work was funded through the University Coal Research Program being administered by DOE-NETL (Award #: DE-FE0026191) and through the National Science Foundation (Grant Number: 1603249).

In memory and honor of my dad

Wish I could crack a cold one with you to celebrate this huge accomplishment of mine, but I know you're always proud of me.

THESIS ABSTRACT

The modeling work and simulation results contained within this thesis come from two different applications that together emphasize multiple of the challenges currently faced by researchers in the field of numerical modeling of gas-solids flows with computational fluid dynamics (CFD) tools, and highlight avenues of potential resolutions to these challenges.

In the first body of work, the MFiX CFD suite, developed by the Department of Energy's National Energy Technology Laboratory (DOE NETL), was utilized to model and simulate several experimental conditions of a fluidized bed (in 2D), and a hopper (in 3D), where solid-solid collision effects play a dominant role. Of concern in these studies are the physical prediction capabilities and associated computational costs of the three different multiphase frameworks available in MFiX: the Discrete Element Model (DEM), the Two Fluid Model (TFM), and the newer hybrid Multiphase Particle in Cell Model (MPIC). Initial selection of an appropriate multiphase modeling framework that satisfies the level of detail and computational cost constraints associated with the problem at hand, is crucial to the successful use of CFD tools in industry. The DEM and TFM frameworks were deemed to be the most accurate in simulating transient pressure profiles in the fluidized bed scenario compared to experimental measurements. TFM framework also proved to be 35% faster. While the MPIC framework was on average 90% faster than the

DEM framework, it failed to produce reasonable predictions of physical flow behaviors. An additional motivation behind this research was to test and explore further reductions in computational costs offered by a recently developed interface of MFiX with the linear solver library, PETSc. Using previously identified numerical strategies in PETSc to solve the pressure equations, a more robust solver convergence behavior than the native pressure solver package was achieved across all three frameworks. Most notably, it enabled the use of larger and fewer time steps in the DEM framework, resulting in a 4-20% reduction in overall solve time to simulate 20 seconds of fluidized bed flow. Despite the significant reduction in computational time, simulation accuracy in terms of predicting the average pressure drop was slightly diminished using the PETSc solver in the DEM framework. Simulations of pure granular flow in a hopper revealed that while the TFM framework experienced difficulties converging the solids pressure term, it was still capable of predicting mass discharge rates that were very similar to those of the DEM framework, but at a comparatively lower computational cost. Again, the MPIC framework predictions differed significantly from the DEM results which are considered the benchmark/gold standard for modeling granular multiphase flows. Thus, despite the significant computational advantages of the MPIC framework over the other two, proper caution needs to be exercised when utilizing it to simulate densely packed solid flows.

In the second body of work, a collection of CFD models and simulations were developed using the ANSYS Fluent DPM framework to simulate air combustion of three different coal types (Powder River Basin (PRB), Illinois #6, and Sufco 2) from select experiments conducted on a pilot-scale combustor from the University of Utah. The

objective of this study was to investigate the sensitivity of ash deposition behaviors to select modeling parameters, with the aim of formulating a particle capture model. Ash formation and deposition is a complex physio-chemical process that negatively affects boiler operation and predicting ash deposit growth rates with CFD modeling techniques is extremely challenging. Many previous attempts by others neglect the importance of adequately resolving the particle size distribution and using an adequate spatial resolution near the heat transfer surface. Combustion modeling methodologies were validated against experimental measurements of flue gas ash concentrations and reactor profiles of temperature, and estimates of velocity. Simulation predictions were deemed to be in satisfactory agreement with experimental measurements. Temperature and velocity profiles were only mildly influenced by the resolutions of both the particle size distribution model and the near-boundary spatial mesh. Simulation predictions for impaction rates on a collector probe boundary were large in comparison to measured values of deposition rates, enforcing the importance of capture efficiency in the effort to accurately predict ash deposit growth rates. Impaction rates also proved to be moderately sensitive to the number of bins used to resolve the particle size distribution, and the degree of this sensitivity was unique to each coal type further emphasizing the challenges in universally modeling combustion and ash deposition across fuel sources. Impaction rates increased significantly when employing a more refined near-boundary mesh which highlights the importance of spatial resolution modeling parameters in successful ash deposition simulation efforts. Additionally, a Weber number criteria capture method was tested across all three coal types and critical Weber numbers were identified in each case

which were significantly different between coal types. These values were found to be much smaller than 1 which signifies the importance of considering attraction forces between the particles and the deposition surface. Predicted deposition rates when applying the critical Weber numbers as capture criteria agreed well with measured values, but demonstrated sensitivity to the number of bins in the particle size distribution model. In the PRB and Illinois coal cases, a mere 10% adjustment in the critical Weber cutoff value resulted in a roughly 30% difference in predicted deposition rates, demonstrating that this method of modeling particle capture is not universal and should be used with caution. Results from this work demonstrate that ash deposition processes are still not fully understood, and the reinforces the need for more collaborative efforts between CFD modelers and experimentalists.

CHAPTER 1

INTRODUCTION

1.1 Motivations and Objectives

Computational fluid dynamics (CFD) modeling and simulation is a major area for scientific research, as rigorously developed models are becoming accepted as valuable problem-solving tools in many industrial settings. In industry, models and simulations have the potential to play an important role in addressing many common industrial problems such as quality and efficiency studies, retrofit and capacity increase projects, and the scale-up of newly designed technologies.

One common and perplexing condition that exists in any industry, from energy to chemical processing, is gas-solids multiphase flows. Recent advancements in the field of CFD research have improved the capacity of understanding surrounding the physical and chemical phenomena exhibited by these flows. Still many challenges remain to develop reliable numerical models capable of solving real world problems. For instance: accounting for collision effects between solids which is even more difficult for irregular particles observed in most real-world particulate phases, and evolving particle size distributions to account for effects like fragmentation which is important in pulverized coal combustion.

The overarching motivation behind the research conducted for the body of this thesis is to build a fundamental understanding of how different modeling approaches attempt to address a select few specific challenges in numerical CFD modeling of multiphase flows. These issues include:

1. Modeling collision effects in *dense* multiphase flow scenarios in a computationally efficient manner
2. Modeling physical phenomena of the ash deposition process in *dilute* multiphase flow scenarios

This work draws and builds upon the work carried out by previous UND ChE graduate students Lauren Clarke and Trevor Seidel.

Lauren Clarke's thesis [1] focused on achieving computational speed-ups in simulating multiphase flows, by interfacing the Department of Energy's National Energy Technology Laboratory's (DOE NETL) open source CFD code MFiX, or Multiphase Flow with Interphase Exchanges, with the linear equation solver library, PETSc to provide enhanced numerical and computational treatments to the pressure solver. The MFiX-PETSc integration was tested on various multiphase flow problems utilizing the Two Fluid Model framework available in MFiX. Solving the pressure correction equation is a well-known bottleneck in multiphase flow simulations and has attempted to be addressed in many other research efforts [2,3]. The MFiX-PETSc integration with the new pressure correction linear equation solver option was found to produce more favorable solve times in certain flow

scenarios involving non-uniform meshes [4]. Chapter 3 of this thesis is an extension of the aforementioned previous work by:

1. Assessing performance improvements offered by the MFiX-PETSc integration across all three multiphase modeling frameworks available in the MFiX CFD suite. These frameworks include the Two Fluid Model (TFM), the Discrete Element Model (DEM), and the Multiphase Particle in Cell (MPIC) model. These models differ in their numerical treatment of solid collision terms with varying degrees of computational speeds and accuracies. This study is undertaken by simulating a fluidized bed scenario with well characterized experimental measurements to enable comparisons of different modeling options.
2. Assessing the performance of the three MFiX frameworks in multiphase flow scenarios where solid collision effects are isolated. This study is carried out by simulating the discharge of solids from a hopper. Hoppers are a ubiquitous unit operation in industry commonly used for handling bulk solids like feedstocks, intermediate materials, and powdered or granular products. Flows discharging from a hopper are dominated by solid-solid and solid-wall interactions and expose the numerical methodologies of each modeling framework.

Studying a dense multiphase flow problem across multiple frameworks as the present work does, provides a unique avenue to highlight both the computational and physical

challenges in modeling collision effects as faced by the field of numerical CFD modeling research.

In the context of dilute, dispersed multiphase flows, Trevor Seidel's thesis [5] focused on predicting and accurately characterizing combustion characteristics and particle dispersion in oxy-coal combustion experiments with two different commercial CFD multiphase frameworks. The end result was an established set of combustion modeling parameters that were capable of accurately describing (in 2D) flame ignition and flame stand-off in conventional combustion and oxy-combustion experiments that were carried out at the University of Utah.

As an evolution of this previous CFD coal combustion modeling work, the goal of the work presented in Chapter 4 of this thesis was to formulate a particle capture model that can reasonably predict growth rates of ash deposits on heat transfer surfaces that agree with well-detailed experimental measurements from the same combustion experimental work from the University of Utah. This is approached by:

1. Carrying out 3D simulations of coal combustion in air of three different coal types using ANSYS Fluent's Discrete Phase Model (DPM). Simulation results were validated against experimental measurements for reactor profiles of temperature and velocity as well as outlet ash concentrations.
2. Assessing the sensitivity of simulation predictions for ash deposition rates to the resolution (number of bins) of the particle size distribution model, highlighting the need

for accurate characterization of the ash particles in ash deposition modeling efforts. Additionally, the sensitivity of ash deposition results to the spatial/mesh resolution near the wall of the deposition probe was also demonstrated.

Ash deposition can cause serious losses in energy efficiency if not controlled properly by engineers, and can be a safety hazard due to its potential to weaken boiler tubes as a result of under-deposit corrosion. In light of this issue, other previous CFD research efforts have demonstrated that adequate characterization of the particle phase and the fluid boundary layers are crucial challenges facing current CFD ash deposition modeling efforts [6–8]. Studying the characterization of the particle phase and boundary layer as they relate to predicting ash deposition in CFD combustion models of different coal types is a novel investigation approach to testing the prospect of certain ash capture sub models.

1.2 Thesis Organization

The collection of work resulting from investigating the motivations described above may be more easily understood if thought of as entirely separate works, as the specific real-world application scenario is different in each problem. However, fundamental lessons learned in each study should not be mistaken as independent conclusions, as these issues each play an equally significant role in the advancement of the field of numerical modeling of complex gas-solid multiphase flows. The chapters and workflow of simulation studies presented in this thesis are organized as follows:

Chapter 2 provides a comprehensive comparison of the different modeling programs/frameworks utilized by discussing the attributes of each one that are important in the research conducted for this thesis. Chapter 2 also further details the generalized format of the governing conservation equations in the two main approaches (Lagrangian and Eulerian) to numerical CFD modeling of gas-solids flows.

Chapter 3 presents the modeling work on solids dense multiphase flows with special attention given to different modeling approaches to resolving collision effects. Two separate sets of experiments, the first on a lab-scale fluidized bed and the second on a bench-scale hopper, conducted by different entities served as the modeling subjects in Chapter 3. Three different experimental conditions of a fluidized bed were modeled in each of the three MFiX frameworks in 2D, with two linear equation solver options for a total of 18 fluidized bed simulations to be compared against each other and validated against experimental data. In the hopper study, two different initial solids loading conditions were modeled in each of the three MFiX frameworks in 3D, for a total of 6 simulations to be compared against each other.

Chapter 4 presents the modeling and simulation analysis work on dilute multiphase flows with special attention given to the physical phenomena of the ash deposition process. Pilot-scale combustion experiments on three different coal types and measurements collected for their respective ash deposition rates served as the modeling subjects in Chapter 4. Three reasonably validated combustion simulations of three coal types were carried out in ANSYS Fluent DPM, and two distinctive sensitivity studies were conducted on select modeling parameters. An additional avenue of research discussed in Chapter 4 is the applicability of a

critical Weber number capture criteria formulation for predicting ash deposition rates. This criteria was also investigated across the same three coal types.

Chapter 5 summarizes the important findings from this work and emphasizes the main conclusions. Chapter 5 also proposes directions for future work that were identified throughout the research efforts pertaining to this thesis.

CHAPTER 2

BACKGROUND

2.1 Basics of CFD Numerical Modeling Methodologies

Over the past few decades, many different modeling approaches have been developed to capture the nature and nuances of multiphase flows. Numerous commercial and open-source CFD codes/software have been rigorously developed and continue to be refined as the CFD research field advances. In this work, multiphase flow models are studied in the open-source code MFiX, developed by the DOE's NETL, and the commercially available ANSYS Fluent. Both of these CFD packages offer multiple different governing multiphase modeling framework options.

Numerical modeling of gas-solids multiphase flows involves the tight coupling of equations governing the physical behaviors and equations modeling the interactions of both the fluid phase and the solid phase. The fluid is generally treated as a continuous phase and is solved by averaging Navier-Stokes equations for conservation of mass, momentum, energy and species. In different multiphase modeling approaches, the governing fluid phase equations are modified appropriately to account for the transfer of mass, momentum, energy, and species from the solids phase. Generally, there are two main approaches to modeling

solids: 1) as a discrete phase and 2) as another continuous phase. In the discrete approach, individual particles are tracked in a Lagrangian frame of reference which means that particle positions in time are tracked in a fixed coordinate system, and their trajectories are calculated while considering impacts by external forces. In the continuous approach, flow characteristics of the solids phase are averaged in a Eulerian domain using special relationships derived from the Kinetic Theory of Granular Flow, and particle dispersion is driven by local gradients. A third type of multiphase model has also emerged more recently which uses a statistical weighting or distribution model to represent more generalized particle properties with Lagrangian tracking abilities, but computes their behaviors and interphase interactions using Eulerian-based methods. Each of these approaches have their advantages and disadvantages depending on the specific problem at hand, and are discussed in more detail in the following sections.

Before going into more detail on the mathematical relationships and technicalities of numerical CFD modeling, a comparison of the different frameworks, and the specific features of each that are considered throughout this thesis, is offered in Table 2.1.

Table 2.1. Summary of multiphase modeling frameworks and their associated features important to the research efforts pertaining to this thesis

Feature	MFiX DEM	MFiX TFM	MFiX MPIC	ANSYS Fluent DPM
General *solids phase* modeling approach	strict Lagrangian	Eulerian	hybrid Lagrangian/Eulerian	hybrid Lagrangian/Eulerian
How collision effects are handled	directly resolved	empirical correlations	empirical correlations	empirical correlations
Range of applicability (current state)	dilute to very dense	dilute to moderately dense	dilute	dilute
Relative computational cost	extremely high	medium	low	low
Solids phase particle size characterization	single, uniform diameter	single, uniform diameter	single, uniform diameter	capable of initial polydispersity but unchangeable throughout simulation

2.2 Detailed Discussion of Lagrangian Approaches (including Mixed Lagrangian-Eulerian Approaches)

In Lagrangian/discrete approaches to modeling a dispersed solids phase, the motion of individual particles is in accordance with Newton's second law along with a collision sub model. In most discrete approaches, direct resolution of individual particle collisions can look like Figure 2.1, and are usually modeled with some modified form of the soft sphere spring-dashpot approach originally developed by Cundall and Strack [9].

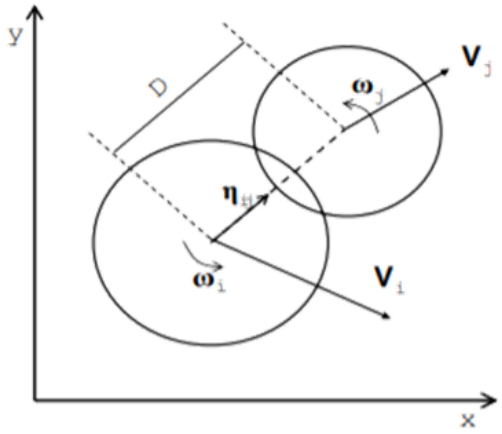

Figure 2.1. Depiction of particle collision modeling in MFiX-DEM (an example of discretely resolving the solids phase) [10]

Strict Lagrangian approaches to particulate modeling possess high fidelity across a wide range of multiphase flow regimes, and can achieve high solids phase resolutions. Some of the advantages of Lagrangian models important to this work are the rigorous development of collision models and drag laws, as well as the ability to consider polydispersity in particle size distributions [11,12]. However, as a result of the high resolution of discrete solids modeling, Lagrangian simulations are often realistically limited to small lab or bench scale sized problems because of the extensive computational effort involved in resolving individual particle behaviors. Parallelization efforts have been attempted to address the computational burden of discrete phase simulations, but are only marginally helpful [13,14]. In realistic problem sizes with trillions of particles, strict Lagrangian tracking discrete phase CFD models are not practical, thus they are mainly reserved for limited comparisons as the gold standard to other numerical modeling techniques to help aid in the development of other less resolved and less computationally expensive methodologies.

Many discrete solids phase models employing a Lagrangian approach actually rely on a hybrid Lagrangian-Eulerian solids phase modeling approach. More efficient calculations are achieved by employing some statistical weighting or distribution model to the individual particles. This methodology was originally constructed by Andrews and O'Rourke [15]. In solids dense flows, a weighting model is typically used to achieve faster solution times by averaging the characteristics of groups of individual particles into gradients within a computational parcel. In dilute applications, hybrid models typically use statistical distribution models to represent the particle phase characteristics and often calculate multiple tracks of one classification of particle in order to diminish the effect of stochastic error introduced by the distribution model. In either situation, the hybrid Euler-Lagrange multiphase modeling approach generally computes phase interactions (i.e. interphase momentum transfer) in the Eulerian fluid frame. The solids phase is still tracked in a Lagrangian frame of reference with governing equations that resemble Equations 2.5-2.8 as discussed below, but the interphase transfers of mass, momentum, and energy are formulated like Equations 2.9-2.17 discussed in the next section.

Despite the computational effort advantages of hybrid Euler-Lagrange multiphase modeling methods, many of these types of models have limited applications due to their empirical assumptions about how the particle characteristics are averaged. MFiX's Multiphase Particle in Cell (MPIC) model, and ANSYS Fluent's Discrete Phase Model (DPM) frameworks are realizations of this methodology. Quantifying the prediction uncertainties in these types of models in order to more rigorously develop the empirical sub-

models for performance across different multiphase flow regimes is an important area of CFD research [16].

Numerically speaking, Lagrangian multiphase models consider both particle-particle interactions and particle-fluid interactions with appropriate modifications to the fluid continuum constituting equations to account for interphase transfers of mass, momentum, energy and species. The particles are tracked in a Lagrangian frame of reference throughout the calculated fluid flow field. Particle track histories can be monitored, and particle dispersion is determined by the fluctuations in turbulent fluid velocities. Examples of the multiphase hydrodynamic governing equations for both the continuous fluid phase and the discrete solids phase with strict Lagrangian tracking are detailed below in Equations 2.1-2.8.

Conservation of Mass in the Continuous Phase:

The generalized equation for conservation of mass, or the continuity equation, in the fluid phase is as follows [17]:

$$\frac{\partial}{\partial t}\left(\varepsilon_g \rho_g\right) + \nabla \cdot \left(\varepsilon_g \rho_g \boldsymbol{v}_g\right) = R_{gm} \qquad \textbf{Eq. 2.1}$$

Where ε_g is the fluid volume fraction, ρ_g is the thermodynamic density of the fluid phase, $\boldsymbol{v}_g$ is the volume-averaged fluid phase velocity, and R_{gn} is the rate of mass addition to the fluid phase from solids phase m.

The fluid density (ρ_g) can be set to a constant value, representing an incompressible fluid, or can be determined with the ideal gas law or another equation of state. The first term on the

left represents the rate of mass accumulation per unit volume, and the second term represents the net rate of convective mass flux. The right-hand side denotes a source term to represent the mass added to the continuous phase from the dispersed solids phase (i.e. reactions).

Conservation of Momentum in the Continuous Phase:

The generalized governing equation for the conservation of momentum in the continuous fluid phase is as follows [17]:

$$\frac{\partial}{\partial t}\left(\varepsilon_g \rho_g \boldsymbol{v}_g\right) = \nabla \cdot \bar{\bar{S}}_g + \varepsilon_g \rho_g \boldsymbol{g} - I_{gm} \qquad \textbf{Eq. 2.2}$$

Where $\bar{\bar{S}}_g$ is the fluid phase stress tensor, $\boldsymbol{g}$ is gravitational acceleration, and I_{gm} represents the momentum transfer between the fluid and solid phases as determined by a separate fluid-particle drag law describing interphase forces.

The first term on the left-hand side represents the rate of change in momentum per unit volume, and the second term represents the rate of momentum change in the fluid phase by convection. The right-hand side terms represent momentum addition per unit volume to the fluid phase by surface forces, body forces (i.e. gravity), and interphase forces, respectively. The fluid phase stress tensor ($\bar{\bar{S}}_g$) accounts for pressure, and viscous shear/strain phenomena in the fluid phase.

Conservation of Energy in the Continuous Phase:

The governing equation for conservation of energy in the fluid phase is as follows [17]:

$$\varepsilon_g \rho_g C_{pg} \left(\frac{\partial T_g}{\partial t} + \boldsymbol{v}_g \cdot \nabla T_g \right) = -\nabla \cdot \boldsymbol{q}_g - H_{gn} - \Delta H_{rg} + H_{wall} \qquad \textbf{Eq. 2.3}$$

Where C_{pg} is the specific heat capacity of the fluid phase, T_g is the thermodynamic fluid temperature, $\boldsymbol{q}_g$ is the fluid phase conductive heat flux, and H is explicit heat transfer, or sensible enthalpy. H_{gn} describes the interphase heat transfer, ΔH_{rg} describes the heat of reactions occurring the fluid phase, and H_{wall} describes the fluid-wall heat transfer.

The left-hand side of the equation represents the rate of change in internal energy per unit volume of the fluid phase and the convective rate of energy transfer. The right-hand side of the equation represents the addition of internal energy to the fluid phase per unit volume due to an external heat flux, interphase transfer, fluid phase reactions, and/or wall conductive heat effects generally described by Fourier's law.

Conservation of Species in the Continuous Phase:

The fluid phase may contain an arbitrary number of chemical species, and if reactions are occurring, the governing conservation equation for species in the fluid phase is as follows [17]:

$$\frac{\partial}{\partial t}\left(\varepsilon_g \rho_g X_{gn}\right) + \nabla \cdot \left(\varepsilon_g \rho_g X_{gn} \boldsymbol{v}_g\right) = R_{gn} \qquad \textbf{Eq. 2.4}$$

Where X_{gn} is the mass fraction of a particular species in the fluid phase, and R_{gn} is the rate of formation of fluid phase species n.

The first term on the left-hand side of the equation represents the rate of change in mass fraction of particular species, and the second term represents the convective transfer of species. The right-hand side of the equation represents the rate of addition of fluid phase species from reactions. Reaction rates can be either kinetic or diffusion limited, or both.

Lagrangian Tracking of the Discrete Phase and Interphase Transfer:

In the discrete approach of dispersed solids phase modeling, each solids phase is represented by an arbitrary number of particles each with a specified diameter and density. Individual particle trajectories are tracked in a Lagrangian frame of reference at time (t) as a function of position, linear velocity, and angular velocity as follows [10]:

$$\frac{\partial}{\partial t}\boldsymbol{X}_i(t) = \boldsymbol{V}_i(t) \qquad \textbf{Eq. 2.5}$$

$$m_i \frac{\partial}{\partial t}\boldsymbol{V}_i(t) = \boldsymbol{F}_{iT} = m_i\boldsymbol{g} + \boldsymbol{F_{iD}}(t) + \boldsymbol{F_{iC}}(t) \qquad \textbf{Eq. 2.6}$$

$$I_i \frac{\partial}{\partial t}\boldsymbol{\omega}_i(t) = \boldsymbol{T}_i \qquad \textbf{Eq. 2.7}$$

Where $\boldsymbol{X}_i$ is the particle position, $\boldsymbol{V}_i$ is the linear velocity of the particle, m_i is the mass of the particle, $\boldsymbol{\omega}_i$ is the angular velocity of the particle, and $\boldsymbol{T}_i$ is the torque force acting on the particle. $\boldsymbol{F}_{iT}$ represents the total force acting on the particle, and is described as the net sum of terms for gravitational, drag ($\boldsymbol{F_{iD}}$), and contact forces ($\boldsymbol{F_{iC}}$). Contact forces account for collision effects, and drag forces account for effects of interphase momentum transfer between the discrete solid and continuous fluid phases.

Interphase momentum transfer can be represented by a variety of scenario specific relationships detailed elsewhere, but is usually determined by some function of the solids volume fraction and Reynolds number [10,18]. The Reynolds number is the ratio inertial to viscous forces in a flow regime and is given by:

$$Re = \frac{\rho_g d_p |\boldsymbol{v}_p - \boldsymbol{v}_g|}{\mu_g} \qquad \textbf{Eq. 2.8}$$

Where d_p is the diameter of the particle, $\boldsymbol{v}_p$ is the particle velocity, and μ_g is the fluid viscosity.

Each discrete solids phase is also subject to governing conservation equations for mass and energy which are similar in form to Equations 2.1 and 2.3. Heat transfer between the fluid and solids phases is often described by scenario specific sub models which can consider various particulate heat transfer phenomena like radiative heat effects in coal combustion, or simple temperature gradient driven interphase heat transfer which can be described by Nusselt number correlations which quantifies the ratio of convective to conductive heat transfer across a phase boundary. Examples of these interphase heat transfer relationships are detailed elsewhere [10,18].

2.3 Detailed Discussion of Eulerian-Eulerian Approaches

Another main approach to modeling a solids phase is employing a Eulerian frame of reference in which the solids phase is treated as a continuum. In this case, the particles of the solids phase move collectively, and collisions are modeled as solids stresses. Usually

Eulerian-Eulerian CFD models are capable of considering both frictional and viscous solids phase forces as depicted in Figure 2.2. Numerical formulations for shearing granular flows commonly employed in these kinds of models was originally developed in part by Schaeffer and built upon further by Jackson and Johnson [19,20]. Eulerian-Eulerian multiphase frameworks are commonly called Two-Fluid models. The basis of a Two-Fluid approach relies on the Kinetic Theory of Granular Flow to provide closure to the momentum conservation equations, and as a result, the solid-fluid drag relationship becomes crucial to the success of Eulerian-Eulerian multiphase models.

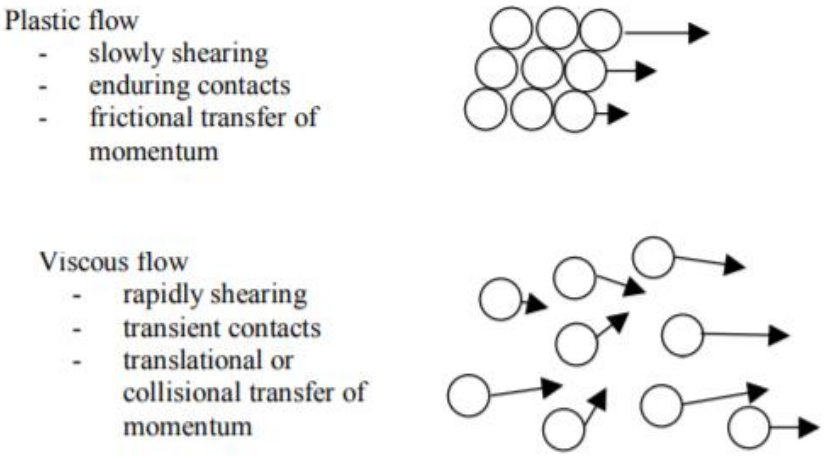

Figure 2.2. Depiction and of frictional and viscous flow regimes exhibited by granular materials adapted from Syamlal et al [17]

By averaging the solids phase like a continuum, computational costs of Eulerian-Eulerian approach simulations are significantly decreased compared to their strict Lagrangian/discrete model competitors. CFD models employing a Two-Fluid approach have demonstrated great promise to be capable of handling large engineering scale problems with

an acceptable degree of certainty, but there are still many challenges to overcome such as addressing the momentum interphase exchange calculation structure and speed [21].

Many CFD researchers have previously attempted to develop robust drag laws to appropriately model the momentum exchange between solids and fluids [22,23]. However, many of these draw laws make far-reaching assumptions about perfect particle sphericity and binary collisions that severely limit the applicability of Eulerian-Eulerian models in certain multiphase flow regimes such as solids dense flows. Similarly, with hybrid discrete models as discussed before, uncertainty quantification studies are an important area of research effort for developing and advancing Two-Fluid models. Another disadvantage of these kinds of models is that individual particle histories cannot be obtained, and attempting to implement advanced particle characteristics like polydispersity can result in computational complexities that begin to outweigh the cost advantages of Eulerian-Eulerian simulations [20].

In Eulerian-Eulerian CFD models, the solids phase is subject to its own conservation equations. The governing conservation relationships detailed below in Equations 2.9-2.17 are shown in terms of the q^{th} continuous phase where the q^{th} phase can be either the solids or fluids phase as the constitutive equations are fundamentally the same.

Conservation of Mass and Species:

The governing continuity equation in a Two-Fluid Model is as follows [17]:

$$\frac{\partial}{\partial t}\left(\alpha_q \rho_q\right) + \nabla \cdot \left(\alpha_q \rho_q \boldsymbol{v}_q\right) = R_{qk} \qquad \textbf{Eq. 2.9}$$

Where α_q is the phase volume fraction, ρ_q is the phase volume-averaged density, $\boldsymbol{v}_q$ is the volume-averaged phase velocity, and R_{qk} is the rate of mass addition to the q^{th} phase from the k^{th} phase.

The first term on the left represents the rate of mass accumulation in the phase per unit volume, and the second term represents the net rate of convective mass flux. The right-hand side denotes a source term to represent the mass added to the continuous phase from either multiphase reactions or an externally defined source. Species are conserved on a mass basis like in Equation 2.4.

Conservation of Energy:

The phase averaged energy conservation equation is as follows [17]:

$$\alpha_q \rho_q C_{pq} \left(\frac{\partial T_q}{\partial t} + \boldsymbol{v}_q \cdot \nabla T_q \right) = -\nabla \cdot \boldsymbol{q}_q - H_{qk} - \Delta H_{rq} \qquad \textbf{Eq. 2.10}$$

Where C_{pq} is the volume-averaged specific heat capacity of the phase, T_q is the volume-averaged phase temperature, $\boldsymbol{q}_q$ is the conductive heat flux, and H is explicit heat transfer, or sensible enthalpy. H_{qk} describes the interphase heat transfer between the q^{th} and k^{th} phases, and ΔH_{rq} describes the resulting heat of reaction from homogenous phase reactions.

The left-hand side of the equation represents the rate of change in internal phase energy per unit volume, and the convective rate of energy transfer. The right-hand side of the equation represents the addition of internal energy to the phase per unit volume generally described by

Fourier's law, due to an external heat flux, interphase transfer, homogenous reactions, and/or wall conductive heat effects.

Conservation of Momentum and Interphase Momentum Exchange Coefficients:

The generalized equation for the conservation of momentum in continuous phases is as follows [17]:

$$\frac{\partial}{\partial t}\left(\alpha_q \rho_q \boldsymbol{v}_q\right) = \nabla \cdot \bar{\bar{S}}_q + \alpha_q \rho_q \boldsymbol{g} - I_{qk} \qquad \textbf{Eq. 2.11}$$

Where $\bar{\bar{S}}_q$ is the phase stress tensor, $\boldsymbol{g}$ is gravitational acceleration, and I_{qk} represents the interphase momentum transfer.

The first term on the left-hand side represents the rate of change in momentum per unit volume, and the second term represents the convective rate of momentum change in the phase. The right-hand side terms represent momentum additions per unit volume to the phase by surface forces, body forces (i.e. gravity), and interphase forces, respectively.

The stress tensor ($\bar{\bar{S}}_q$) in a continuous phase is given by [17]:

$$\bar{\bar{S}}_q = -P_q \bar{\bar{I}} + \bar{\bar{\tau}}_q \qquad \textbf{Eq. 2.12}$$

Where P_q is the phase averaged pressure, $\bar{\bar{I}}$ is the identity tensor, and $\bar{\bar{\tau}}_q$ is the stress-strain tensor. In a fluid phase, $\bar{\bar{\tau}}_q$ describes shear stress and shear strain phenomena observed in fluids.

In a continuous solids phase, the stress tensor ($\bar{\bar{\tau}}_q$) is derived from granular flow theory which describes both viscous and plastic solids flow regimes and a solids pressure term is calculated to keep solids phase void fraction from becoming less than it is in a packed bed of the granular solids [17].

The interphase momentum exchange term denoted by I_{qk} in Equation 2.11 is particularly important in the governing relations of Two-Fluid models. This term is generally described by a solids-fluid drag law derived specially for continuous phase calculations, and are usually a function of some interphase exchange coefficient resembling the form [12]:

$$\boldsymbol{F}_D = \beta\left|\boldsymbol{v}_s - \boldsymbol{v}_g\right| \qquad \textbf{Eq. 2.13}$$

Where $\boldsymbol{F}_D$ is the fluid-solids drag force, and β is an arbitrary interphase exchange coefficient.

The Syamlal-O'Brien drag law, used in the simulations discussed in Chapter 3, models the interphase exchange coefficient as follows [24]:

$$\beta = \frac{3}{4}\frac{C_D}{{V_{rs}}^2}\frac{\rho_g \varepsilon_g \varepsilon_s \left|\boldsymbol{v}_s - \boldsymbol{v}_g\right|}{d_p} \qquad \textbf{Eq. 2.14}$$

Where C_D is the drag coefficient given by:

$$C_D = \left(0.63 + \frac{4.8}{\sqrt{Re_p/V_{rs}}}\right)^2 \qquad \textbf{Eq. 2.15}$$

In Equation 2.14, V_{rs} is an empirical correlation detailed elsewhere, for the ratio of terminal settling velocity of a multi-particulate system to that of a single particle, which is a function of the particle Reynolds number (Re_p), the gas and solids volume fractions ($\varepsilon_g, \varepsilon_s$), and two tuning parameters; a and b [24].

The Morsi-Alexander drag law, used in the simulations discussed in Chapter 4, models the interphase exchange coefficient as follows [18]:

$$\beta = \frac{C_D Re}{24} \qquad \textbf{Eq. 2.16}$$

Where C_D is the drag coefficient given by:

$$C_D = a_1 + \frac{a_2}{Re} + \frac{a_3}{Re^2} \qquad \textbf{Eq. 2.17}$$

Where the three a's are numerical values that adjust as a stepwise function of the local Reynolds number (Re) over a comprehensive range of Reynolds numbers [25].

REFERENCES (CHAPTERS 1 & 2)

[1] Clarke L. Interfacing The CFD Code MFiX With The PETSc Linear Solver Library To Achieve Reduced Computation Times. University of North Dakota, 2018.

[2] Chandran K, Muralidhar K. Condition number analysis of flow fields arising from CFD simulations. Int J Adv Eng Sci Appl Math 2018;10:238–51. https://doi.org/10.1007/s12572-018-0230-0.

[3] Hua J, Lou J. Numerical simulation of bubble rising in viscous liquid. Journal of Computational Physics 2007;222:769–95. https://doi.org/10.1016/j.jcp.2006.08.008.

[4] Clarke LE, Krishnamoorthy G. Pre-conditioning strategies to accelerate the convergence of iterative methods in multiphase flow simulations. Mathematics and Computers in Simulation 2019;165:200–22. https://doi.org/10.1016/j.matcom.2019.03.009.

[5] Seidel TL. Predicting Flame Stability, Ash Deposition And Radiative Heat Transfer Characteristics During Oxy-Fuel Combustion Of Pulverized Coal Using Different Multiphase Modeling Frameworks. University of North Dakota, 2019.

[6] Weber R, Schaffel-Mancini N, Mancini M, Kupka T. Fly ash deposition modelling: Requirements for accurate predictions of particle impaction on tubes using RANS-based computational fluid dynamics. Fuel 2013;108:586–96. https://doi.org/10.1016/j.fuel.2012.11.006.

[7] Cai Y, Tay K, Zheng Z, Yang W, Wang H, Zeng G, et al. Modeling of ash formation and deposition processes in coal and biomass fired boilers: A comprehensive review. Applied Energy 2018;230:1447–544. https://doi.org/10.1016/j.apenergy.2018.08.084.

[8] Krishnamoorthy G, Wolf C. Assessing the Role of Particles in Radiative Heat Transfer during Oxy-Combustion of Coal and Biomass Blends. Journal of Combustion 2015;2015:1–15. https://doi.org/10.1155/2015/793683.

[9] Cundall, Strack. The Distinct Element Method as a Tool for Research in Granular Media. National Science Foundation; 1978.

[10] Garg R, Galvin J, Li T, Pannala S. Documentation of open-source MFIX–DEM software for gas-solids flows n.d.:40.

[11] Chen S, Adepu M, Emady H, Jiao Y, Gel A. Enhancing the physical modeling capability of open-source MFIX-DEM software for handling particle size polydispersity: Implementation and validation. Powder Technology 2017;317:117–25. https://doi.org/10.1016/j.powtec.2017.04.055.

[12] Agrawal V, Shinde Y, Shah MT, Utikar RP, Pareek VK, Joshi JB. Effect of drag models on CFD–DEM predictions of bubbling fluidized beds with Geldart D particles. Advanced Powder Technology 2018;29:2658–69. https://doi.org/10.1016/j.apt.2018.07.014.

[13] Bakshi A, Shahnam M, Gel A, Li T, Altantzis C, Rogers W, et al. Comprehensive multivariate sensitivity analysis of CFD-DEM simulations: Critical model parameters

and their impact on fluidization hydrodynamics. Powder Technology 2018;338:519–37. https://doi.org/10.1016/j.powtec.2018.06.049.

[14] Liu P, Hrenya CM. Challenges of DEM: I. Competing bottlenecks in parallelization of gas–solid flows. Powder Technology 2014;264:620–6. https://doi.org/10.1016/j.powtec.2014.04.095.

[15] Andrews M, O'Rourke P. The multiphase particle-in-cell (mp-pic) method for dense particulate flows. International Journal of Multiphase Flow 1996;22.

[16] Gel A, Garg R, Tong C, Shahnam M, Guenther C. Applying uncertainty quantification to multiphase flow computational fluid dynamics. Powder Technology 2013;242:27–39. https://doi.org/10.1016/j.powtec.2013.01.045.

[17] Syamlal M, Rogers W, O`Brien TJ. MFIX documentation theory guide. 1993. https://doi.org/10.2172/10145548.

[18] ANSYS Fluent Theory Guide (19.1). ANSYS Inc. Online Manual Resource; Release 19.1.

[19] Schaeffer DG. Instability in the Evolution Equations Describing Incompressible Granular Flow. Journal of Differential Equations 1987;66.

[20] Johnson PC, Jackson R. Frictional-Collisional Constitutive Relations for Granular Materials with Application to Plane Shearing. Journal of Fluidi Mechanics n.d.;176.

[21] Moliner C, Marchelli F, Bosio B, Arato E. Modelling of Spouted and Spout-Fluid Beds: Key for Their Successful Scale Up. Energies 2017;10:1729. https://doi.org/10.3390/en10111729.

[22] Gidaspow D. Multiphase flow and fluidization : continuum and kinetic theory descriptions. Boston: Boston : Academic Press; 1994.

[23] Syamlal M, O' Brien TJ. Fluid dynamic simulation of O 3 decomposition in a bubbling fluidized bed. AIChE Journal 2003;49:2793–801. https://doi.org/10.1002/aic.690491112.

[24] Syamlal M, O'Brien TJ. The Derivation of a Drag Coefficient Formula from Velocity Voidage Correlations n.d.:20.

[25] Morsi SA, Alexander AJ. An investigation of particle trajectories in two-phase flow systems. Journal of Fluid Mechanics 1972;55:193–208. https://doi.org/10.1017/S0022112072001806.

CHAPTER 3

Dense Multiphase Flows: Assessing the Numerical and Computational Performance of Different Collision Modeling Methodologies

Abstract:

In order to alleviate the stringent computational demands of multiphase CFD tools and increase their adoption by industry, the present work assesses the computational costs and accuracies of three solid collision modeling methodologies within the open source CFD code MFiX (Multiphase Flow with Interphase Exchanges): the Discrete Element Model (DEM), the Two Fluid Model (TFM), and the newer hybrid Multiphase Particle in Cell (MPIC) Model. The DEM and TFM frameworks were deemed to be the most accurate in simulating transient pressure profiles from a well-characterized experimental fluidized bed, and the TFM framework proved to be 35% faster. While the MPIC framework was on average 90% faster than the DEM framework, it failed to produce reasonable predictions of transient pressure profiles in a pseudo-2D fluidized bed. A recently developed interface of MFiX with the linear solver library, PETSc, was also tested to explore further reductions in solve times across all three frameworks. Using previously identified numerical strategies in PETSc (BiCGSTAB with Block Jacobi preconditioning) to solve the pressure equations, a more robust solver convergence behavior than the native pressure solver package was

achieved across all three frameworks. Specifically, it enabled the use of larger and fewer time steps in the DEM framework, resulting in a 4-20% overall reduction in solve times to simulate 20 seconds of a fluidized bed compared to using the native MFiX solver. However, some simulation accuracy was lost using the PETSc solver in the DEM framework. Simulations of a 3D pure granular flow hopper revealed that while the TFM framework experienced difficulties converging the solids pressure term, it was still capable of predicting mass discharge rates, at a reasonable computational cost, that were very similar to those of the DEM framework. Again, the MPIC framework predictions differed significantly from the DEM predictions which are considered to be the gold standard benchmark for granular multiphase flows. Thus, despite the significant computational advantages of the MPIC framework over the other two, proper caution needs to be exercised when utilizing it to simulate densely packed solids flows.

3.1 Introduction

Dense solids-gas flows, where the volume fraction of solids is on the order of 10%, are commonly encountered in many industrial operations like pneumatic transport of bulk solids, drying of granular materials, and fluidized bed reactors. Numerical and computational methods for modeling and simulating these kinds of flows can be valuable tools to serve engineers with better insights to their unusual flow behaviors and help to better predict and control them. With the progressive development of CFD modeling and simulation packages, several challenges have surfaced in the context of both the physical and numerical constraints

of certain approaches. In this thesis chapter, solids dense multiphase flows in a lab scale fluidized bed, and a bench scale hopper, are studied across multiple numerical CFD frameworks available in the DOE National Energy Technology Laboratory's open-source CFD code suite, MFiX (Multiphase Flow with Interphase Exchanges). This work aims to investigate the competencies of the different framework approaches to resolving collision effects in flow scenarios where they are isolated, and highlight the computational challenges that arise.

3.1.1 Physical Challenges in Modeling Dense Multiphase Flows

As discussed previously in greater detail in Chapter 2, there are two main approaches to numerical modeling of multiphase flows: Lagrangian(solids)-Eulerian(fluids) and Eulerian(solids)-Eulerian(fluids). In the Lagrangian approach for modeling solids, collisions are resolved for each individual particle or small parcels of individual particles. The MFiX-DEM framework, or the Discrete Element Model, is a realization of multiphase CFD modeling with strict Lagrangian reference to particle collisions. Discrete solids simulations are capable of resolving simultaneous collisions and thus possess high fidelity and accuracy in dense multiphase flow scenarios, especially in 3D. However, tracking individual particles requires a great deal of computational effort, rendering discrete particle simulations unpractical for industrial scale problems even with parallel computing capabilities [1,2]. Despite their computational burdens, Lagrangian/discrete simulations are highly revered for

their prediction accuracies, especially in dense multiphase flow scenarios and are important for helping to test and improve other, more efficient, frameworks.

One way of addressing the large computational requirements of Lagrangian simulations is to consider groups of individual particles, known as parcels, since resolving individual particle behaviors is usually more detail than necessary. This research front has led to the development of hybrid Lagrangian-Eulerian solids phase models, where a weighting or probability function is employed to represent groups of individual particles with more generalized characteristics. The hybrid multiphase modeling framework in MFiX is called the Multiphase Particle in Cell (MPIC) model, or MFiX-MPIC and is the newest available framework in the MFiX suite.

Hybrid multiphase modeling methodologies do help alleviate computational costs but lack the rigorous development that strict Lagrangian tracking approaches have experienced over time. Many hybrid multiphase models are semi-empirical and make assumptions that limit their applications to dilute flows. Thus, an important area of CFD research is quantifying prediction uncertainties in Lagrangian-Eulerian models over a wide range of applications in order to improve the empirical model structures and parameters. One of the pressing challenges in using these kinds of hybrid models is selecting an optimal weighting factor as this requires a very detailed level of understanding of the physical characteristics of the real particles, and both the numerical and computational domains of the problem. Others have previously investigated the importance of this weighting factor in multiphase flow regimes, and their results have enforced the known fact that selecting the parcel weighting

factor requires a delicate balancing of desired solids volume fraction, mesh density and overall solids mass. Some researchers have even attempted to functionalize the relationship between these modeling parameters, but the challenge still remains [3].

In the Eulerian approach to multiphase modeling, the solids phase is modeled as an interpenetrating continuum along with the fluid phase, and momentum transfer is governed by the Kinetic Theory of Granular Flow. Averaging the solids phase inherently provides Eulerian-Eulerian simulations a great computational cost advantage over strict Lagrangian methods. However the sub models can become extremely computationally extensive to capture desired nuances of solids flows which may negate this advantage. Modeling the gas-solids drag forces is one of the main challenges currently facing the progression of Two-Fluid models. Drag laws in Eulerian-Eulerian approaches are often empirical which can severely limit the applicability of TFM simulations to certain flow regimes of certain solids densities. Many of these models are still in development requiring more rigorous validation and quantification studies especially in solids dense flow scenarios. Similar in name to other models of its kind, the Eulerian-Eulerian framework available in MFiX is called the Two Fluid Model (TFM).

Validated and robust TFM simulations can provide valuable insights about multiphase hydrodynamics at promising reduced computational costs compared to their discrete element counterparts. However, there exists a known bottleneck in TFM simulations involving the numerical solving of the pressure correction equation that can hinder their computational advantage. This challenge is also apparent in MPIC simulations as collision

effects are calculated in a similar manner to the interphase momentum exchange in the Eulerian computational frame. Addressing this pressure solve bottleneck in these kinds of simulations is currently being vigorously addressed by the CFD research community [4,5].

3.1.2 Numerical Challenges in Modeling Dense Multiphase Flows

The TFM and MPIC frameworks in MFiX are considered more efficient at modeling collision effects compared to DEM models, however they are taxed by the known simulation bottleneck arising from solving the pressure correction equation derived for solving the momentum conservation equations in dynamic multiphase CFD modeling. Briefly stated, the pressure correction issue can be described as the numerical and computational difficulty in calculating and converging the pressure correction matrix, which determines the realistic momentum transfer between the solids and fluid phase continuums. One way of addressing this issue was studied by previous UND ChE graduate student, Lauren Clarke. As a result, the 2016.1 version of the MFiX source code was altered and equipped with access to an additional suite of more robust and scalable numerical solvers available in PETSc, a suite of high powered computational tools developed by the DOE's Argonne National Laboratory [6]. The resulting MFiX-PETSc integration was tested for computational and physical performance in a variety of multiphase flow scenarios, to determine the best preconditioner and solver combinations to reduce the overall computational effort required to converge the pressure correction equation to a specified tolerance every time. The new treatments to the pressure solver (BiCGSTAB with Block Jacobi preconditioning) were found to produce 28-

40% faster solution times than the native MFiX solver (BiCGSTAB with line preconditioning) in fine mesh cases modeled in the TFM framework depending on the discretization scheme [7]. The motivation behind the work presented in this chapter is to further test the PETSc solver performance in all three MFiX frameworks.

The exact details of how the code modifications affect the numerical and computational solving process in MFiX CFD simulations can be found in elsewhere [7] and are not of importance in this work. The results from this previous work shall be referred to herein as the PETSc pressure correction equation solver option available in all MFiX frameworks. The PETSc solver is unique to the originally built-in native solver, which is still used to solve the mass and energy conservation equations in the simulations in this work. Both solvers are held to the same residual tolerance standards, which means that both solvers must iteratively converge the pressure correction equation solutions to a specified residual balance every time.

The numerical performance metric of interest in this work is the overall computational cost, or time to solution as experienced by a user, and can be represented in a functional form as follows:

$$C_o = (N_{i_P} * dt) + C_e \qquad \textbf{Eq. 3.1}$$

Where, C_o refers to the overall computational cost per simulation time unit, or the number of CPU seconds required to calculate 1 second of simulation time. In this relationship, N_{i_P} represents the number of inner iterations of the pressure correction

equation per time step, dt represents the number of time steps per simulation second, and C_e represents all other necessary computational costs, per simulation time step, that are external to solving the pressure correction equation.

With specific regard to collision effects and the pressure solve issue with Eulerian simulations, the most important factors influencing overall computational cost of a simulation include:

1. The number of inner iterations required to converge the pressure correction term to a specified residual tolerance each computational time step
2. The number of computational time steps it takes to solve/reach the desired simulation time
3. Additional computational costs external to solving the pressure term including the initial cost of setting up the matrix structures, and more importantly, the work required to resolve and compute collision effects

The MFiX CFD code evokes an adaptive time stepping method that either reduces or increases the time step between outer iterations based on how well the governing equations are solved as indicated by their overall outer iteration residuals. This means that a user would only observe a decrease (comparative) in overall computational cost, or overall solve time, if a combination of any of the following are significantly true:

a) The pressure solver performed more efficiently by reducing the number of inner iterations in a time step required to converge to the same tolerance each time

b) The pressure solver performed more robustly by iteratively converging on a better/more stable/more realistic solution that allows for quicker convergence of the outer iterations of the other governing equations to a specified residual tolerance, ultimately allowing for larger time steps

c) The general effort taken to setup the computational schemes and resolve/compute collision effects was reduced by an external factor/modeling methodology parameter

The relationship between and importance of these components of computational performance is not very well understood by CFD researchers. Previous but mainly separate efforts have been made to quantify the importance of solving the pressure term and degree of collision resolution, in the speed and accuracy of dense multiphase flows, but these efforts were mainly focused in one particular framework at a time [8,9]. Assessing and comparing the numerical performances of multiple frameworks side by side, as this work aims to do, is a rather unique lens for contributing to the research and development efforts in the field of multiphase CFD modeling.

3.2 Description of Dense Multiphase Flow Experiments

The main objective of the work presented in this chapter was to establish a collection of models and simulation cases across all three MFiX-CFD frameworks (DEM, MPIC, and TFM) that reasonably model the solids dense multiphase flow regimes observed in a fluidized bed and in a granular hopper. Comparative analysis of the validity of predicted collision effects and computational/numerical effort performances, across all three frameworks may provide valuable insight to challenge areas in CFD modeling.

Two sets of physical experiments were identified to serve as the subjects for this study: 1) a lab scale fluidized bed from researchers at the National Energy Technology Laboratory, and 2) a bench scale hopper from researchers at Arizona State University [10,11]. These experiments were selected based on the availability of detailed measurements to help ascertain confidence in the modeling methodologies of this work and to verify reasonable simulation predictions. Modeling these scenarios provides a comprehensive view of the physical and computational performance of the MFiX frameworks with regard to collisions by isolating their effect by varying the solids fractions, including pure granular flow. In the case of granular flow, fluid phase calculations were disabled, which provides an even more isolated view of the differences in approaches to collision modeling between each of the frameworks and their influence on solving the pressure correction equation. The details of each set of experiments as they pertain to the focus of this work are explained in the following sections.

3.2.1 NETL'S Fluidized Bed Challenge Problem

In NETL's Small Scale Challenge Problem I (SSCPI) [10], researchers released detailed measurements and steady state pressure profile results from experiments on a rectangular fluidized bed of nylon beads in air. A list of particle properties can be found in Table 3 and a diagram of the facility can be seen in Figure 3.1. The fluidized bed apparatus is 122 cm tall, 23 cm wide, and 7.6 cm deep. The fluid, which is simply ambient air, is pumped into a distributor plate that distributes the air flow evenly across the entire cross-sectional area of the bottom inlet face. The nylon beads were initially poured in to form a naturally settled packed bed with a height of 16.5 cm.

Table 3.1. Physical properties of the nylon beads used in the fluidized bed experiments from NETL's Small Scale Challenge Problem I [12]

Property	**Measured Value**	**Units**
Diameter	3.256	mm
Density	1131	kg/mm^3
Minimum fluidization velocity (u_{mf})	1.05	m/s
Packed bed void fraction	0.4	
Initial bed height	16.5	m
Sphericity	0.94	

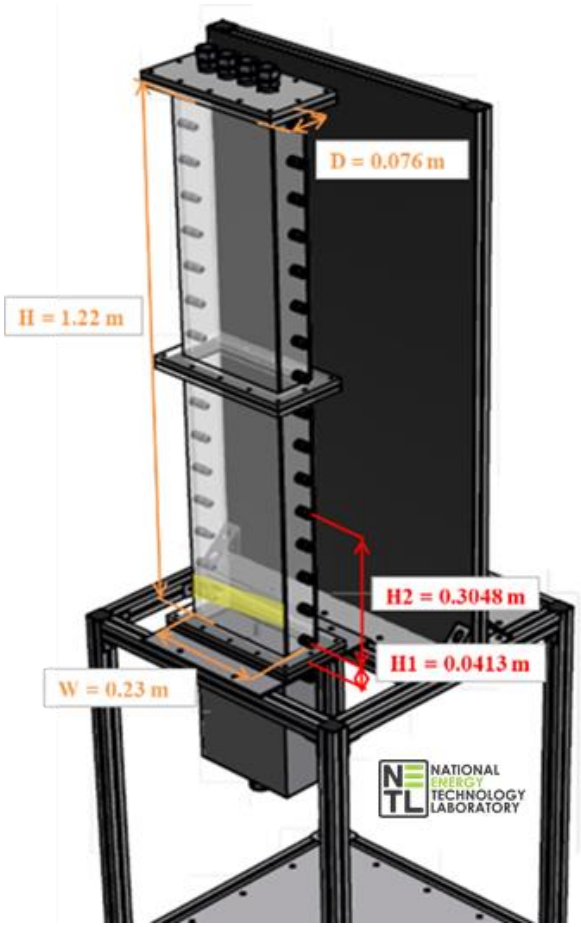

Figure 3.1. Diagram of the experimental fluidized bed apparatus used in experiments from NETL's Small Scale Challenge Problem I [10]

Pressure was measured with a fast response pressure transducer at the two ports indicated by H1 and H2 in Figure 3.1. The instantaneous difference between these measurements was recorded over time for fluid velocities of 2.19 m/s, 3.28 m/s and 4.38 m/s, or 2, 3 and 4 times the determined minimum fluidization velocity of the bed. For clarity in comparing cases later, these inlet velocities will herein be referred to as low, medium, and high. The average and RMS values for the axial pressure drop between the two ports at each

fluid velocity were selected as the validation result of interest for this work, and are reported in Table 3.2.

It is important to note that in a later report released from the party responsible for these experiments, it was stated that they believed instrumentation bias may have significantly influenced the originally reported results [18]. Thus, a more generous than usual simulation prediction accuracy (~10% is generally considered acceptable) is reasonable for the fluidized bed simulation cases presented in this work.

Table 3.2. Reported statistics on pressure drop measurement results from fluidized bed experiments in NETL's Small Scale Challenge Problem I [13]

Inlet Fluid Velocity (m/s)	**Average Axial Pressure Drop (kPa)**	**RMS of Average Axial Pressure Drop (kPa)**
2.19 ($2u_{mf}$)	0.69	0.18
3.28 ($3u_{mf}$)	0.65	0.32
4.38 ($4u_{mf}$)	0.50	0.23

3.2.2 ASU'S Hopper Discharge Problem

In a separate set of physical experiments, researchers at Arizona State University were interested in studying the discharge dynamics and segregation effects in a cylindrical hopper, which had also previously been studied in similar fashion by researchers at Purdue University [11,14]. The goal of the ASU study was to enhance the modeling capabilities of the MFiX-DEM CFD framework by implementing the numerical and computational

capability to consider bi-modal polydispersity in the solid phase. They conducted experiments in a bench-scale hopper with two different types of silica beads, each with a purposefully unique size distribution. The main results presented consider the discharge of a well-mixed bed of the two bead types, and a layered initial configuration.

The physical bench-scale hopper used in the ASU discharge experiments is pictured below in Figure 3.2. Table 3.3 outlines the physical properties of the two bead types as reported by the experimenters. The hopper is 17.3 cm in height and 12.5 cm in width at the widest point. The main cylinder piece is 12.5 cm tall with a diameter of 12.5 cm, with a cone of 3.5 cm tall at a 55º cone angle, and the bottom short cylinder outlet is 1.3 cm tall with a diameter of 2.5 cm. Two different silica bead types were utilized, each with a unique particle size distribution and average particle diameter of 0.29 cm and 0.15 cm, respectively.

Figure 3.2. Image of the physical hopper used in experiments on discharge dynamics from Arizona State University [11].

Table 3.3. Physical properties of two silica bead types from hopper discharge experiments performed at Arizona State University [11].

	Property	Measured Value	Units
Bead Type #1	Particle diameter (average)	0.29	cm
	Particle density	2.5	g/cm^3
	Spring constant	$2.5x10^5$	g/s^2
	Friction Coefficient	0.5	
	Coefficient of restitution	0.9	
	Total initial mass	580	g
Bead Type #2	Particle diameter (average)	0.15	cm
	Particle density	2.5	g/cm^3
	Spring constant	$2.5x10^5$	g/s^2
	Friction Coefficient	0.5	
	Coefficient of restitution	0.9	
	Total initial mass	420	g

In the ASU hopper experiments, the hopper was filled with an arbitrary configuration of a specific mass of each particle type, as listed in Table 3.3, to a height of approximately 8.5 cm above the cone. This yields a solid fraction of 0.53 (void fraction of 0.47) based on the average particle diameters. The sides of the hopper were coated with an anti-static solution before the beads were gently poured into the hopper and the naturally packed bed was leveled at the top. Once the bed was settled, the bottom of the hopper was opened and allowed to freely discharge until empty. A batch sampling method was used to obtain data about the discharge rate and mass fractions of each bead type over the entire discharge time period.

3.3 Modeling Methodologies

The MFiX suite contains three different frameworks for multiphase CFD modeling, all of which are utilized in this work: DEM, MPIC, and TFM. More details on the explicit governing equations of each framework can be found in the MFiX documentation guides [15–17].

MFiX contains several drag relationship options. Drag correlations for fluidized beds were previously studied by Musango et al [18], and it was found that the Syamlal O'Brien drag law, as detailed in Chapter 2, gave the best simulation predictions in the flow regime of interest. Thus, this correlation was selected as the drag law to be used in all the fluidized bed and hopper models presented in this chapter.

As a result of using a weighting model methodology in the MFiX-MPIC framework, an important piece in executing successful MFiX-MPIC simulations is selecting an appropriate statistical weighting factor. In the modeling work presented in this chapter, the statistical weighting factor used in both the fluidized bed and hopper simulations in the MPIC framework was set equal to 5.0. This value was initially identified from previous modeling research by Li et al [3] on a fluidized bed in a similar hybrid framework, and proved to be adequate in both the fluidized bed and hopper MPIC models in this work. Adoption of an appropriate statistical weighting factor is indicated by minimal discrepancy between the desired and actual initialized particle numbers which is discussed as a result of each study.

3.3.1 Fluidized Bed Modeling Methods

The NETL SSCPI fluidized bed experiments were modeled using MFiX-PETSc 2016.1 in the DEM, MPIC and TFM frameworks at the low, medium, and high fluid velocities, and utilizing both the native and PETSc pressure equation solvers for a total of 18 models and simulation cases.

A pseudo-2D geometry was created to model the NETL SSCPI fluidized bed experiments, as pictured in Figure 3.3. The geometry is 122 cm tall and 23 cm wide just like the physical apparatus, but is only as deep as the diameter of a particle. Previous simulations of the NETL SSCPI also conducted in 2D, were found to give comparable results for pressure prediction profiles as 3D simulations, and naturally require less time to solve [13].

The side walls were all set to non-slip boundary conditions such that velocities near the wall diminish in the boundary layer. The bottom of the bed was set to a uniform inflow boundary condition at the desired inlet fluid velocity (y-direction) in each case, and the top of the bed was set as a pressure outflow boundary condition at atmospheric pressure. The air was modeled with a constant density and viscosity of 1.21 kg/m^3 and 0.000018 kg/ms. During post processing of the simulation results, pressure values were extracted from a point in the middle of the geometry at 4 and 35 centimeters in height as indicated in Figure 3.3.

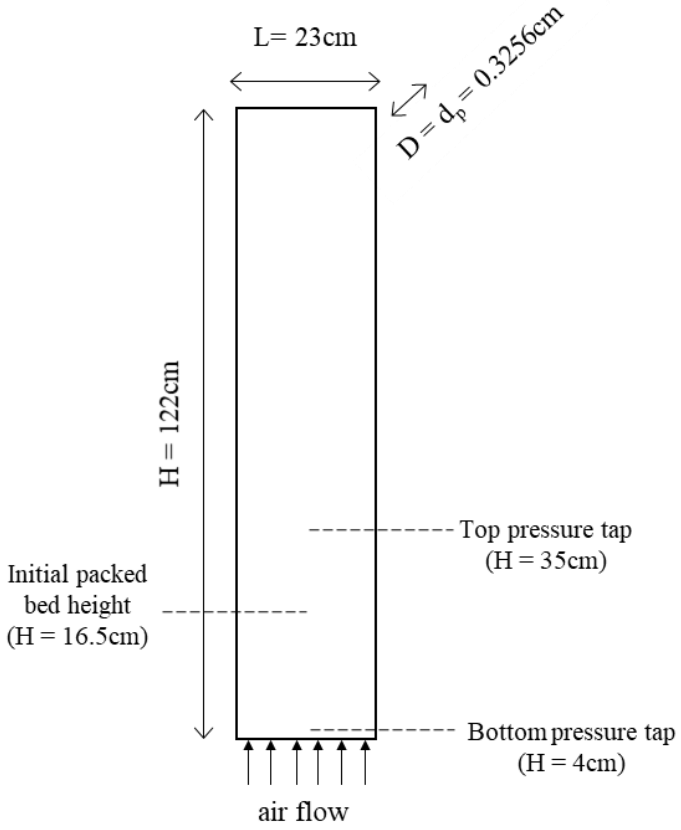

Figure 3.3. Pseudo-2D geometry designed to model the fluidized bed experiments in NETL's Small Scale Challenge Problem I

In each simulation case, the geometry was initialized with a solids bed approximately 16.5 cm high with a void fraction of 0.4 as reported by the experimenters. In the pseudo-2D geometry in this work, this results in approximately 4,100 actual particles. The geometry was fit with a uniform mesh of resolution 1 cell = 1 cm, which is approximately 3 times the diameter of a particle.

The nylon particles were modeled as a solids phase of uniform diameter and density of 0.003256 m and 1131 kg/m^3 respectively, as measured by the experimenters. Additional

details of the modeling parameters used in each framework are summarized in Tables 3.4-3.6. Values for the coefficients of Coulombic friction (resulting from two solid granules in dry contact) and restitution were adopted from measurements on particle-particle interactions directly from the experimenters. The solids stresses model in the MPIC framework is more generalized as particle-particle collisions are not directly resolved, thus the coefficients were simply averaged.

Each simulation was set to run for 20 seconds in order to capture several seconds of steady-state behavior, and the numerical parameters summarized in Table 3.7 remained consistent throughout all the cases. The maximum number of iterations was set at a very large number in order to force all linear solver solutions to converge to the specified tolerances.

Table 3.4. Summary of MFiX-DEM framework CFD modeling details used in all 2D fluidized bed DEM cases

Parameter/Phenomena	**MFiX CFD-DEM Model**	**Reference**
Collisions	Linear Spring Dashpot Model	[17]
Particle-Particle		
Normal spring constant	800 N/m	[19]
Friction coefficient	0.35	[12]
Restitution coefficient	0.84	[12]
Particle-Wall		
Normal spring constant	800 N/m	[19]
Friction coefficient	0.35	[12]
Restitution coefficient	0.92	[12]

Table 3.5. Summary of MFiX-MPIC framework CFD modeling details used in all 2D fluidized bed MPIC cases

Parameter/Phenomena	MFiX CFD-MPIC Model	Reference
Number of particles per parcel	5	[3]
Collisions	MPPIC Frictional Stress Model	[16]
Particle-Particle		
First frictional coefficient of restitution	0.6	
Second frictional coefficient of restitution	0.6	
Particle-Wall		
Restitution coefficient	0.92	[16]

Table 3.6. Summary of MFiX-TFM framework CFD modeling details used in all 2D fluidized bed TFM cases

Parameter/Phenomena	MFiX CFD-TFM Model	Reference
Viscous stress model	Algebraic	[17]
Drag law	Syamlal-O'Brien	
	a=0.87	[19]
	b=2.12	[19]
Frictional stress model	Schaeffer	[17]
Particle-Particle		
Restitution coefficient	0.84	[12]
Packed bed void fraction	0.4	[12]
Angle of internal friction	30º	[18]
Particle-Wall		
Restitution coefficient	0.92	[12]

Table 3.7. Summary of important numerical model parameters applied to all 2D fluidized bed cases

Numerical Modeling Parameter	Specified Value
Stop time	20 s
Initial time step	0.001 s
Maximum number of iterations	10,000
Residual tolerance (outer)	0.001
Linear equation tolerance (inner) *(pressure equation)*	0.001
discretization method *(pressure equation)*	First-Order Up-Winding

3.3.2 Hopper Modeling Methods

The ASU hopper discharge experiments were modeled in 3D in the 2019.1 release of MFiX which offered a more user-friendly geometry wizard, and substantial improvements to the MPIC framework compared to the 2016 version in which the MPIC framework had been implemented in the code, but had not yet been validated. The intention behind developing these models though, is to translate them into the MFiX-PETSc integration version of MFiX in future work to further investigate the capabilities of the PETSc solver in granular flows. Thus, the modeling work and simulations presented in this thesis focus on establishing the crude preliminary groundwork to successfully modeling the ASU discharge experiments in future work.

In both the editions of the MFiX CFD code used to conduct the work in this thesis, a single solids phase, is restricted to characterization by a single uniform particle diameter. This is true in all three frameworks. Considering this limitation, the most realistic model of

the ASU experiments would require two solids phases, which was found to be difficult to initialize in 3D across all three MFiX frameworks in a consistent manner. Subsequently, the ASU hopper discharge experiments were modeled as homogenous beds of each particle type, in each of the three MFiX frameworks, for a total of six models and simulations. The beads from the ASU experiments were modeled as separate solids phases with uniform particle diameters equal to the average diameters reported by the experimenters previously presented in Table 3.3.

A 3D geometry of a cylindrical hopper, as pictured in Figure 3.4, was created to model the ASU hopper discharge experiments. The geometry consisted of a cylinder with a radius of 6.25 cm and 12.5 cm in height attached to a cone with a vertical height of 3.5 cm that converges from a radius of 6.25 cm to 1.25 cm where it attaches to a small cylinder with a radius of 1.25 cm and a height of 1.5cm. Another larger cone diverges into a larger cylinder that is 15.5 cm in height with a radius of 6.25 cm. The geometry was fit with a rectangular mesh 38 cells in the y direction and 14 cells in the x and z directions. This is approximately 3 times the diameter of the larger particles.

The bottom collection cylinder was made large enough to catch and hold the discharged particles without interfering with the mass coming out of the hopper itself. The purpose for the inclusion of the collector was simply to provide a simulation postprocessing region to analyze the properties of the discharged particles for future modeling efforts with multiple particle sizes and solids phases.

All surfaces of the hopper geometry were set as non-slip boundary conditions, including the bottom of the collector bin. The top of the hopper was set as a pressure outflow boundary at atmospheric pressure. The yellow region in Figure 3.4 indicates the initial particle region where particles were automatically generated by MFiX according to the specified void fraction and particle properties defined. The initial void fraction was set to 0.47 in all of the hopper cases to model the settled packed beds from the ASU experiments. As each MFiX framework approaches modeling collision effects differently, they also approach the initialization process differently as well, and the particle initialization results from the hopper simulations in this work will be discussed later in section 3.4.3.

Tables 3.8-3.10 outline in more detail the specific modeling parameters used in the hopper discharge cases in each of the three MFiX frameworks. The empirical parameters for the MPIC collision model were adapted from the MPIC hopper tutorial created by the developers of MFiX that was released with the 19.2 edition of the software.

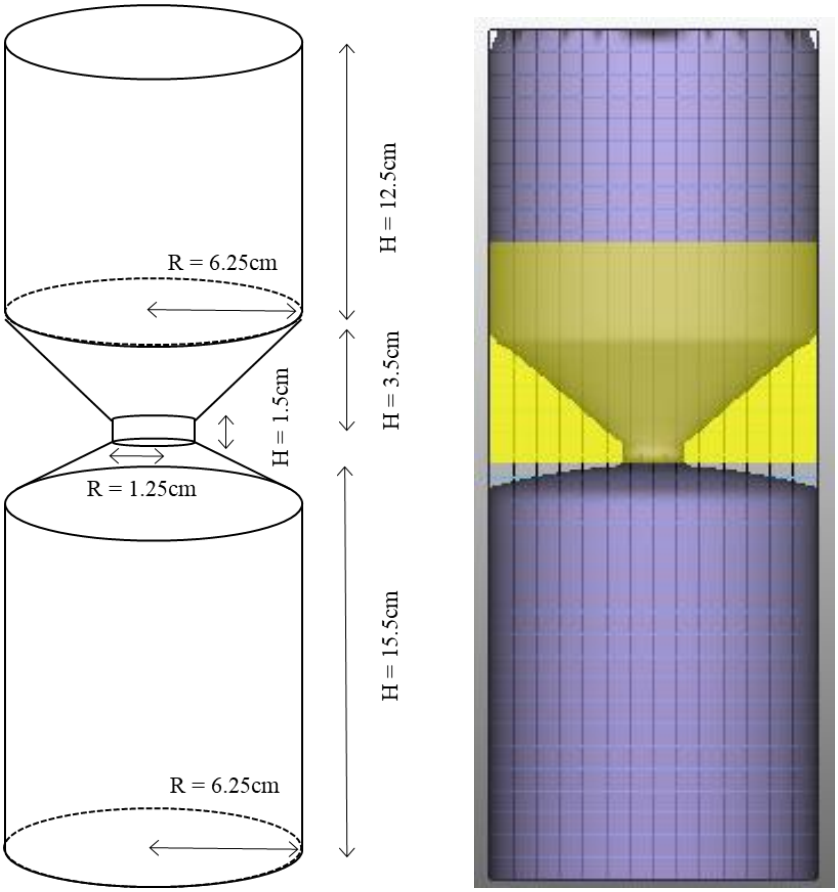

Figure 3.4. 3D geometry employed in all hopper discharge cases designed to model the ASU experiments. The drawing on the left includes dimensions, and the image on the right depicts the initial bed region (yellow) and the mesh size relative to the geometry.

All of the hopper discharge models presented in this work are pure granular flow models meaning that the fluid phase is disabled, and the only governing equations considered are those of the solids phase as uniquely approached by the different frameworks. Each simulation was run until all of the solids emptied from the initial region.

Table 3.8. Summary of MFiX-DEM framework CFD modeling details used in all 3D hopper discharge DEM cases

Parameter/Phenomena	MFiX CFD-DEM Model	Reference
Collisions	Linear Spring Dashpot Model	[17]
Particle-Particle		
Normal spring constant	250 N/m	[11]
Friction coefficient	0.5	[11]
Restitution coefficient	0.9	[11]
Particle-Wall		
Normal spring constant	250 N/m	[11]
Friction coefficient	0.5	[11]
Restitution coefficient	0.9	[11]

Table 3.9. Summary of MFiX-MPIC framework CFD modeling details used in all 3D hopper discharge MPIC cases

Parameter/Phenomena	MFiX CFD-MPIC Model	Reference
Number of particles per parcel	5	
Collisions	MPPIC Frictional Stress Model	[16]
	Empirical dampening factor = 0.85	
	Solids-slip velocity scale factor = 1	
Particle-Wall		
Coefficient of restitution	0.9	[11]

Table 3.10. Summary of MFiX-TFM framework CFD modeling details used in all 3D hopper discharge TFM cases

Parameter/Phenomena	MFiX CFD-TFM Model	Reference
Viscous stress model	Algebraic	[17]
Drag law	Syamlal Obrien	[20]
	a=0.87	[19]
	b=2.12	[19]
Frictional stress model	Schaeffer	[17]
Particle-Particle		
Restitution coefficient	0.9	[11]
Packed bed void fraction	0.47	
Angle of internal friction	30^{o}	
Particle-Wall		
Restitution coefficient	0.9	[11]

3.4 Results and Discussion

The results of the work presented in this chapter compare and assess simulations of dense solid-gas flows across three solid collision modeling frameworks: Two Fluid Model (TFM), Discrete Element Model (DEM) and Multiphase Particle in Cell (MPIC) Model. Such a comparative analysis (across the three frameworks), has not been done to date and is the novel aspect of this study. There are three important forces that a solid experiences in these scenarios: 1) fluid-solid drag forces which are modeled in an identical manner across all three frameworks, 2) solid-solid collisions which are modeled differently in each framework, and 3) solid-wall collisions which are modeled differently in each framework.

The goal of this chapter was to explore how the different frameworks perform (in terms of cost and accuracies) in two scenarios:

- Fluidized bed (where fluid-solid drag forces may dominate the solid-solid or solid-wall forces). In the fluidized bed scenario, experimental measurements were available to assess fidelities
- Hopper (where there is virtually very little fluid-solid drag such that solid-solid and solid-wall interactions are dominant). In the hopper scenario, measurements of discharge rates were not available. However, the computationally expensive DEM framework which is held as the "gold standard" in modeling these flows due to its ability to resolve each individual particle-particle interaction accurately, was considered as “benchmark data” for comparison purposes in this scenario. The geometric scale and the number of particles (~$4x10^3$ particles) within the hopper were chosen to enable the computationally expensive DEM simulations to be carried out in a reasonable amount of time.

In both the fluidized bed and hopper simulations, each framework produced unique results both physically and computationally which speaks to the fundamental differences in the solids phase collision modeling approaches taken by the three frameworks available in the MFiX CFD suite. Results from the fluidized bed study are discussed first, followed by the results of the granular flow hopper study.

In the fluidized bed study, the first main result is the validity and accuracy of the simulation predictions for bubbling behaviors, and the dynamic pressure profile fluctuations

that are attributed to fluidized beds in steady state. The remaining fluidized bed study results focus on the overall computational cost metric which spotlights the numerical and computational traits and challenges associated with each framework and assesses the performance of the PETSc solver.

In the hopper study, the main result of interest is the mass discharge rate predictions. Since no experimental measurement was available from the ASU work for homogenous beds, the results of this study from each framework are simply compared directly between each other. The solids phase initialization performance of each framework is also discussed.

3.4.1 Fluidized Bed Pressure Profile Prediction Results

Initial impressions of the general steady-state multiphase fluidization patterns in all 18 cases appeared consistent with experimental observations of mild bubbling characteristics observed at lower velocities with slugging fluidization behavior approached at higher velocities and thus were deemed satisfactory. Figure 3.5 displays the visual difference in the height of the fluidized bed (represented by the void fraction of air) at each inlet fluid velocity in the TFM simulations for illustrative purposes. While only the TFM simulation results are shown, the bulk bed heights were comparable between all three frameworks and consistently increased with increasing inlet velocities within each of the DEM and MPIC framework simulations as well. This demonstrates that all three frameworks agreed upon adequately capturing the gas-solid fluidization behaviors.

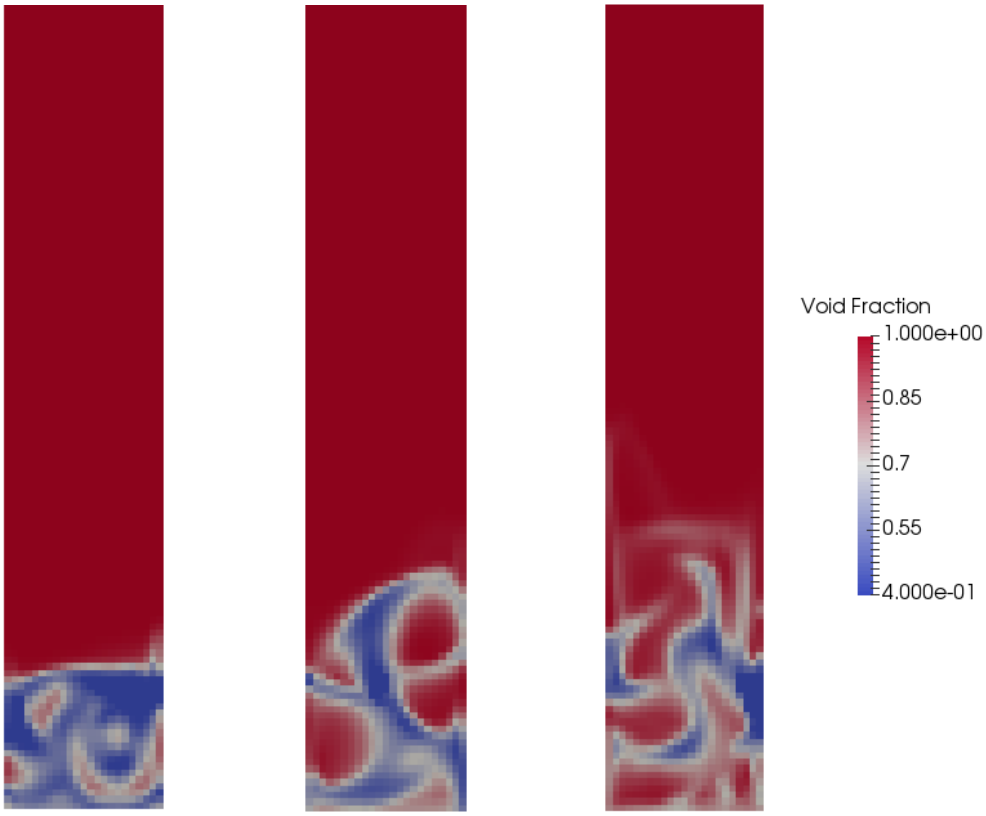

Figure 3.5. Comparative visualization of relative fluidized bed heights (represented by the void fraction of air) as inlet fluid velocity increases in the TFM simulations (native MFiX linear solver)

Figure 3.6 illustrates the visual differences in the solids phase modeling approaches by each framework. Each simulation in the DEM framework employed the same user-defined initial particle configuration with exactly 4,104 particles, and the automatic particle generation function used in the MPIC framework simulations resulted in 1,840 computational parcels which each represent the averaged behavior of 5 real particles. This discrepancy is also apparent in the overall average (area and time averaged) void fraction in the simulation cases pictured in Figure 3.6, which was 0.88 in both the DEM and TFM framework

simulations, and 0.86 in the MPIC framework simulation. While this disparity is relatively small and unlikely to significantly affect the pressure profile predictions, this observation highlights the challenge of selecting an appropriate parcel weighting factor when setting up multiphase simulations in the MPIC framework.

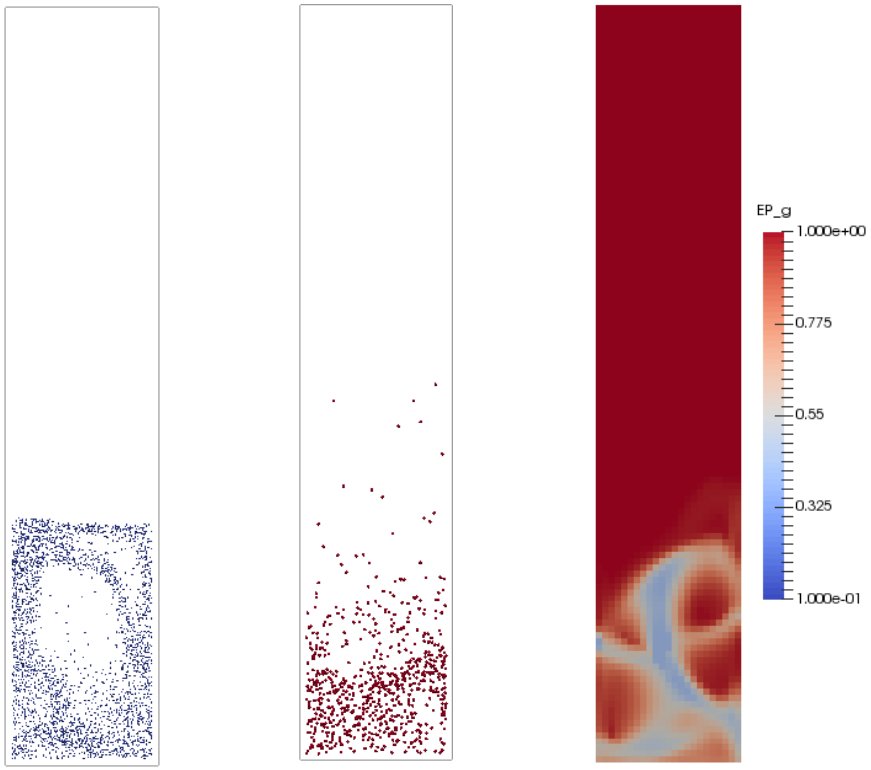

Figure 3.6. Comparative visualization of bubbling patterns and relative fluidized bed heights from simulation results (native MFiX linear solver) at the medium inlet velocity for**: a)** DEM framework, **b)** MPIC framework, and **c)** TFM framework

Figure 3.7 shows how experimental measurements for the instantaneous pressure drop across the bed over time compare to the fluctuating pressure profiles as predicted by each framework. Generally, each framework was still capable of predicting pressure profile fluctuations roughly within the limits of the experimental measurements, but the

characteristic differences in the results in Figure 3.7 exemplify the fundamental differences between the frameworks with regard to modeling collision effects. The DEM framework, which considers simultaneous individual particle collisions, predicted the most accurate fluctuating pressure profile that agrees well with the experimental average and standard deviation limits. The MPIC framework struggled to accurately model the frictional collision effects in the more densely packed areas near the bottom of the fluidized bed, thus resulting in a smaller instantaneous pressure differential prediction. This speaks to the assumptions that the MPIC framework relies on, and exposes the shortcomings in modeling solids dense multiphase flow scenarios of the current state of the MFiX-MPIC solids stresses models. The TFM framework predicted a more appropriate fluctuating pressure profile than the MPIC framework, and only slightly over predicted the pressure differential as observed in Figure 3.7. This demonstrates that the MFiX-TFM sub models used in this study, particularly the drag law, are likely appropriate for modeling this dense multiphase flow regime, but would require further parameter fine-tuning to improve results.

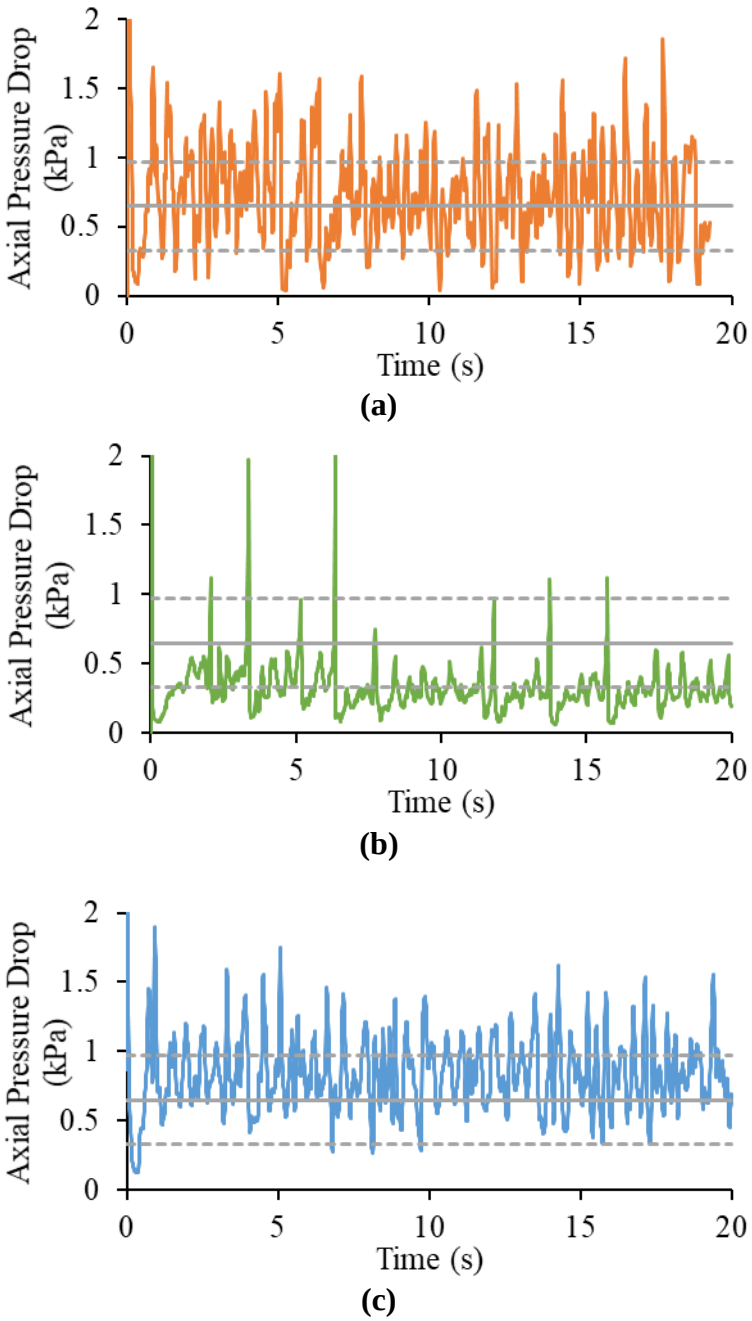

Figure 3.7. Simulation prediction results (native MFiX linear solver) for instantaneous axial pressure drop (between heights of 4 cm and 35 cm) over time at the medium inlet fluid velocity for: **a)** DEM framework, **b)** MPIC framework, and **c)** TFM framework *(grey lines represent the average pressure drop from the experimental measurements; dashed lines represent one standard deviation above and below the mean respectively)*

The results of the fluidized bed study that have been discussed to this point, focused on the simulation cases employing the native linear solver for solving the pressure correction equation (BiCGSTAB with Block Jacobi preconditioning). In all three frameworks, the native linear solver for the pressure correction equation gave satisfactory results that were within experimental limits for fluctuating bed pressure profiles considering some of the limiting modeling assumptions made (i.e. 2D, coarse uniform mesh, non-slip walls) and given the wavering confidence in the experimental measurements from Musser et al [21]. In future work, these models can be further refined with sensitivity studies on different modeling parameters such as mesh resolution and wall treatments, but the current results were good enough to begin exploring the PETSc solver.

Next, given that the solution to the pressure-correction equation is often the "bottleneck" in simulating multiphase flows, the suite of linear solver and preconditioners in PETSc were explored to see if they would expedite the multiphase simulations while retaining the fidelities of the native MFiX linear solvers. Before comparing the computational performance, it was first necessary to ascertain that the MFiX interface with the PETSc linear solver library was working correctly.

Figures 3.8-3.10 summarizes the validation results and prediction accuracies of the PETSc solver. Within the TFM framework, the PETSc solver predicted average pressure profile results that were almost identical to those of the native solver indicating that the interface was working correctly. This suggests that simulation accuracy using the PETSc

solver could similarly be improved like results using the native solver would be with more detailed model development and assumption testing in future work.

Results from Figure 3.8 also show that in the DEM framework, the PETSc solver actually reduced the accuracy of simulation predictions for average bed pressure drop compared to the native solver predictions and the experimental measurements, especially in the medium velocity case. The PETSc solver in the DEM framework performed the best in the high velocity case, producing an average bed pressure drop within the experimental measurement limits. These results warrant further investigation of the PETSc solver in the DEM framework to test for further depreciation or improvements in simulation accuracy in fluidized beds and other solids dense flow regimes.

In the MPIC framework, the PETSc solver also produced inconsistent results compared to the already poor predictions of the native solver. However, the pressure profile prediction accuracy of the PETSc solver in the MPIC framework appears to increase with increasing fluid velocity. This demonstrates that the current approaches to multiphase modeling in the MFiX-MPIC framework are currently more applicable in dilute flows, and also indicates that the PETSc solver might have the potential to improve simulation accuracy in the MPIC framework. However, when the PETSc linear solver was interfaced with the MPIC and DEM frameworks, considerable prediction variations were observed between the native linear solver in MFiX and the PETSc linear solver. MFiX employs an adaptive time-stepping scheme were the time-step size for advancement in a simulation is determined by the rate of convergence of the linear solvers. The difference in predictions among the linear

solvers in Figures 3.9 and 3.10 indicate that the PETSc linear solver convergence characteristics significantly altered the time-stepping behavior of the MPIC and DEM frameworks. This will be clear in the ensuing discussion and warrants further investigation in the future.

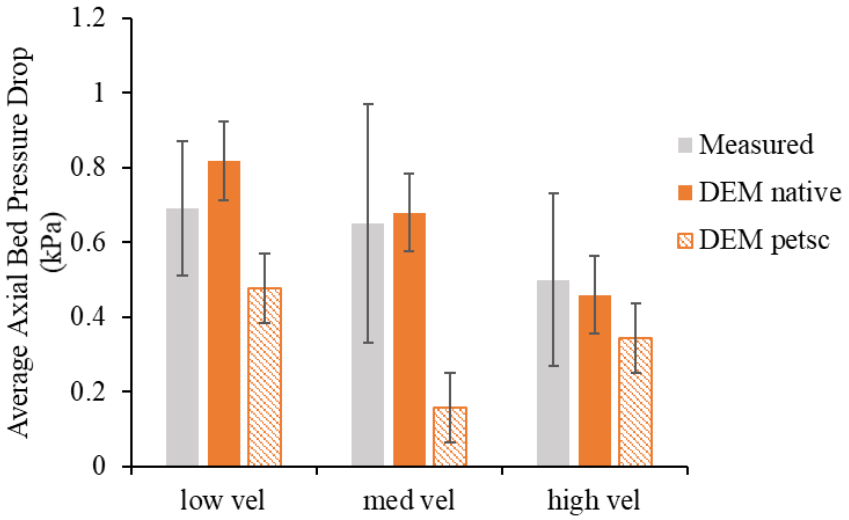

Figure 3.8. Comparative results over inlet fluid velocities for average axial pressure drop predictions from each solver case in the DEM framework

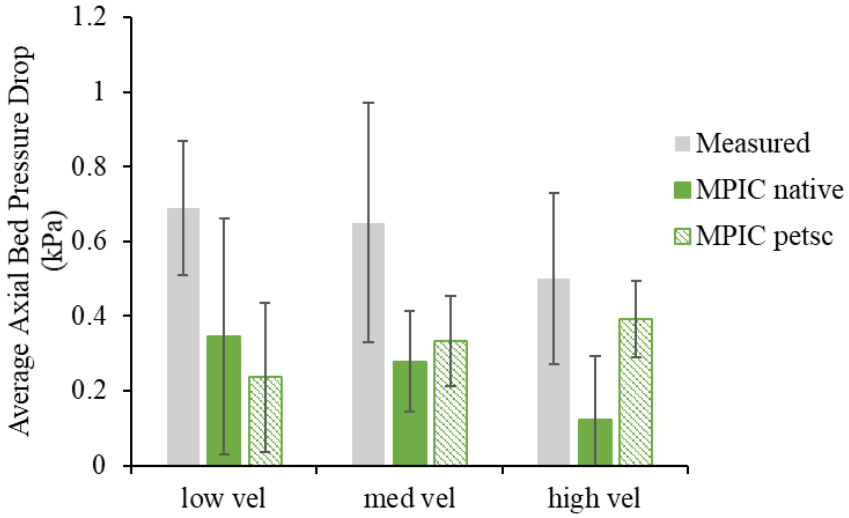

Figure 3.9. Comparative results over inlet fluid velocities for average axial pressure drop predictions from each solver case in the MPIC framework

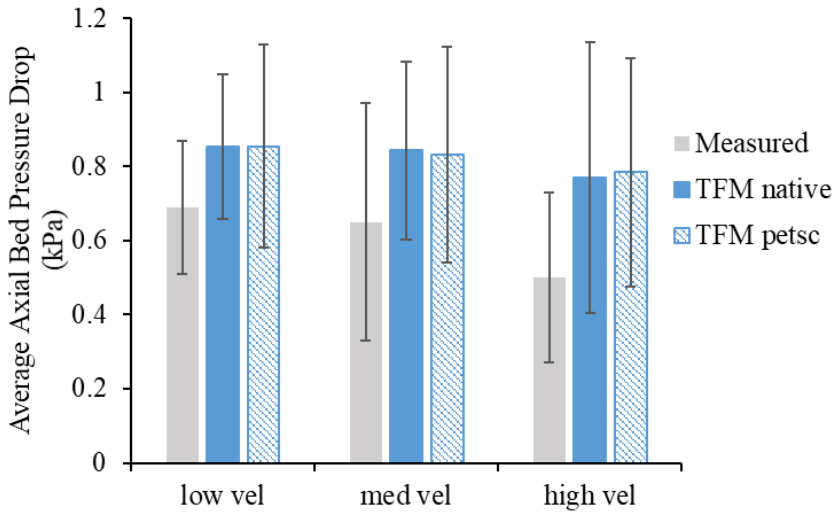

Figure 3.10. Comparative results over inlet fluid velocities for average axial pressure drop predictions from each solver case in the TFM framework

3.4.2 Fluidized Bed Computational Performance Results (PETSc Solver)

As explained in Section 3.1.2, overall computational cost is an important variable of interest in this work. Table 3.11 summarizes the overall time to solution required for 20 seconds of simulation in each of the 18 modeling cases. Simulations in the DEM framework required the most time, followed by the TFM framework cases, and the MPIC framework cases had the lowest, most desirable computational costs. The TFM and MPIC frameworks were, on average, 35% and 89% faster than the DEM simulations, respectively.

The PETSc solver successfully decreased overall computational costs slightly in the DEM framework through reductions in the number of time-steps to achieve 20 seconds of simulation. However, the use of larger step-sizes resulted in a loss of fidelity as shown in Figure 3.8. As anticipated, the PETSc solver did not decrease the computational costs in the

TFM and MPIC framework cases in this work because they employed a uniform computational mesh.

Table 3.11. Outline of overall computational effort required for 20 seconds of simulation in each modeling case

Total Simulation Solve Time (CPU hours)							
	Velocity:	Low		Medium		High	
Pressure Equation Solver:		native	PETSc	native	PETSc	native	PETSc
Framework:	**DEM**	9.03	8.65	8.59	6.91	6.96	6.62
	MPIC	1.20	1.98	0.90	1.40	0.55	1.03
	TFM	6.00	10.32	4.93	10.30	4.92	9.99

The PETSc solver was exclusively evoked to solve only the pressure correction equation pertaining to the governing momentum conservation equation, thus one of the first results to analyze is the importance, or weight, of the converging of the pressure equation in each framework. This can be represented by comparing the ratio of the total solve time between analogous cases using the PETSc and native solvers, to the ratio of the average inner iterations in each case that were required for the pressure solver to converge the solution to the same specified tolerance each time step. Figure 3.11 depicts these results. Points lying close to a slope of unity would suggest that the overall computational effort in that simulation case is highly correlated with the computational effort required solely by the pressure equation. Points lying further away from the line indicate that some other computational cost effect (such as the overhead associated with constructing and assembling the matrices and vectors or the cost of solid collision modeling) are more influential.

It is apparent that external computational costs in the DEM framework are significant. This reinforces the fact that resolving collision effects on an individual particle basis demands considerable computational effort. This means that either of the other two variables in Equation 3.1 must be the source of the overall decrease in computational cost observed using the PETSc solver in the DEM framework.

Figure 3.11 also illustrates the crucial bottleneck in TFM and MPIC simulations caused by the pressure correction equation. The blue and green circle data points, which indicate the low velocity cases in the TFM and MPIC frameworks, lie almost directly on the line, and as the inlet fluid velocity increases, the triangle and square points move further and further away. This trend indicates that the pressure solve bottleneck is most dominant in higher solids density flow regimes, which highlights the incentive to devote research to attacking the pressure solve bottleneck challenge in Eulerian-like multiphase models. This result also indicates that MPIC simulations in MFiX are equally challenged by this problem as TFM simulations.

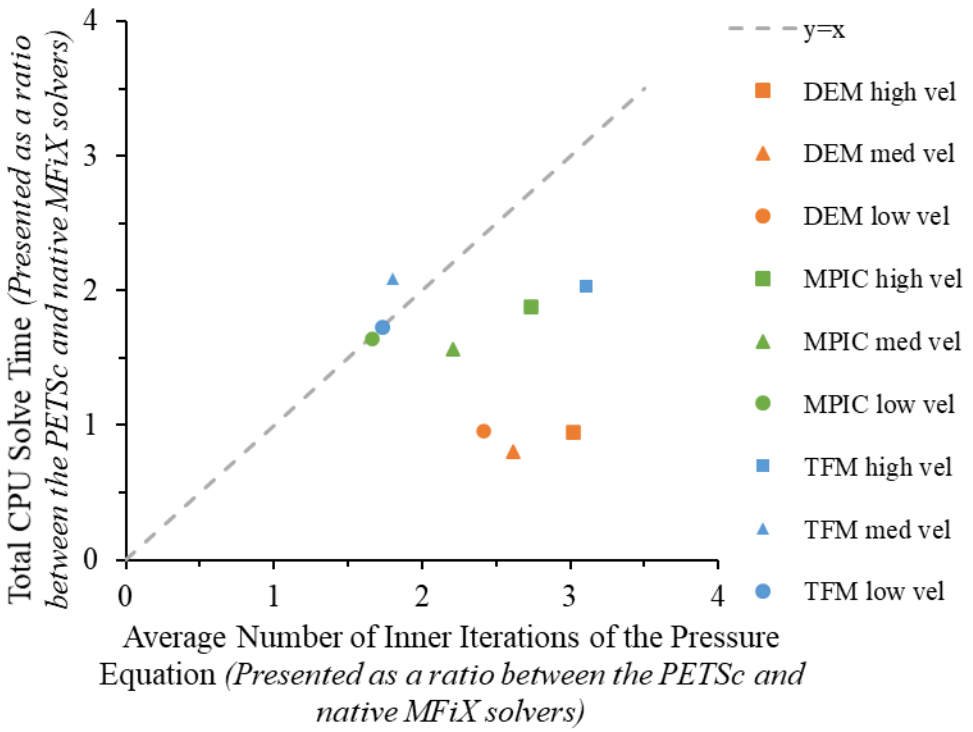

Figure 3.11. Correlation of normalized computational effort (PETSc/native ratio in analogous modeling cases) between the pressure equation solution and the overall solution

Further investigating the remaining two pieces of computational cost in Equation 3.1 that are specific to solving the pressure equation, Figure 3.12 depicts the efficiency of the PETSc solver, and Figure 3.13 depicts the robustness. In Figure 3.12, the average number of inner iterations of the pressure equation required per time step to converge it to the same specified residual tolerance each time, is normalized by the ratio between the PETSc and native MFiX linear solver cases. In this graph, all of the ratios across all three frameworks are greater than 1. This means that the PETSc solver, on average, required roughly twice as many iterations to converge the linear equation corresponding to the pressure correction equation to a tolerance of 0.001 compared to the native solver originally built into MFiX.

This is true even in the DEM framework, which means that the solver efficiency does not explain the reduction in overall computational time observed when using the PETSc solver.

The total number of time steps required to compute 20 seconds of simulation time in each case, as a facet of MFiX's adaptive time step feature, is presented in Figure 3.13 as the normalized ratio between the analogous PETSc and native solver cases. Results from Figure 3.13 show that the ratio is less than 1 in the MPIC and DEM frameworks. This result awards credibility to the robustness of the PETSc solver, and indicates that the unique numerical and computational treatments it provides to the pressure equation improve performance in terms of precision and stability. In the DEM and MPIC frameworks, the ratio is well less than 1, and is likely the source of the observed overall computational cost improvement. However, this utilization of larger time step-sizes resulted in a loss of fidelities as shown in Figures 3.8 and 3.9. This compelling conclusion was interesting, and will guide future work further investigating the capabilities of the PETSc solver in other modeling conditions.

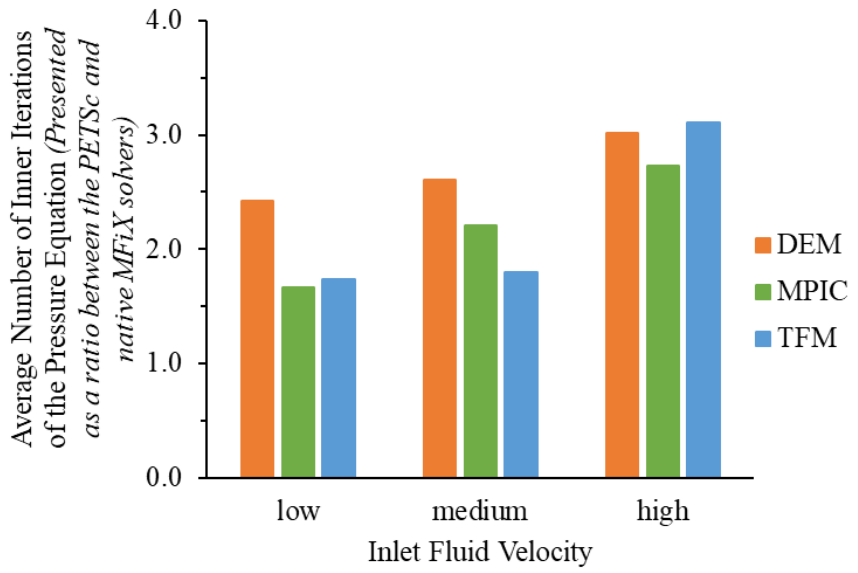

Figure 3.12. Normalized ratio (PETSc/native) of the average number of inner iterations per time step required by the pressure solver to converge the pressure equation to a specified inner residual tolerance

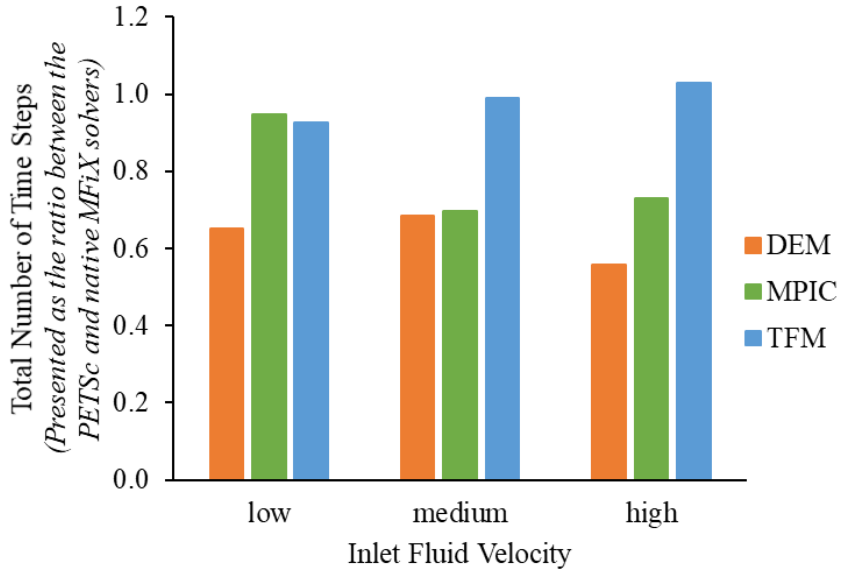

Figure 3.13. Normalized ratio (PETSc/native) of the total number of time steps required to converge 20 simulation seconds to a specified outer iteration residual tolerance

3.4.3 Hopper Discharge Rate Prediction Results

Directly comparing the hopper discharge simulation results between the frameworks revealed noticeable differences between the solids phase modeling approaches in each of the frameworks. Figure 3.14 provides typical snapshots of discharge rates during the simulations of the three frameworks side by side. Table 3.12 presents the total computational effort in CPU hours required by each of the simulations. The MPIC and TFM frameworks proved to be significantly faster than the DEM framework once again, even in 3D pure granular flow scenarios.

It is important to note that both of the TFM hopper simulations experienced difficulties converging, mainly due to converging the solids pressure variable which is important to the solids stress model employed by the TFM framework. Several attempts were made to address the issue including increasing the specified residual tolerance levels, applying different discretization schemes, and adjusting the mesh resolution, but total convergence of the TFM simulation of the larger particles was unable to be fully achieved. Thus, some of the results presented for this simulation case have been projected and/or estimated based on partial draining of the hopper. Achieving full convergence is a challenge that CFD modelers are often faced with when attempting to conduct and successful TFM simulations, and is a notable disadvantage that hinders the progression of Eulerian-Eulerian models in industry and should continue to be addressed by CFD researchers and developers.

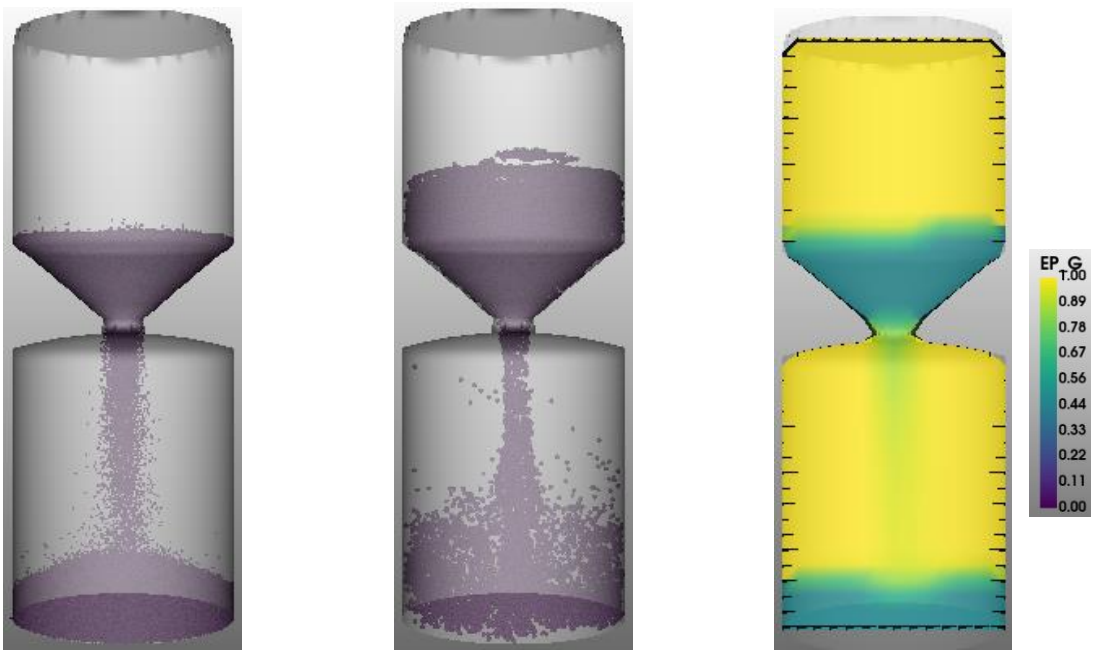

(a) **(b)** **(c)**

Figure 3.14. Visual comparison of hopper discharge simulation results at 3 seconds of the smaller particle (type #2) cases for: **a)** DEM framework, **b)** MPIC framework, and **c)** TFM framework (vertical slice)

Table 3.12. Computational effort required to simulate complete emptying of the initial bed in each hopper case

Case		Solution Time to Empty (CPU hours)	Normalized Computational Effort (CPU hour/Simulation second)
Larger Particles (Type #1)	**DEM**	12.5	1.73
	MPIC	0.10	0.01
	TFM	7.5 *(projected)*	0.88 *(projected)*
Smaller Particles (Type #2)	**DEM**	85.1	15.8
	MPIC	0.69	0.05
	TFM	3.55	0.54

The void fraction of the initial solids region was monitored over time in each hopper discharge simulation case in order to assess the discharge dynamics predicted by each framework. The results are shown in Figure 3.15 in terms of the solids fraction for all six cases. The first important result from Figure 3.15 is how different the predictions of the MPIC framework are from those of the DEM and TFM frameworks. The total time to empty predicted by the MPIC framework was generally 2-3 times longer than the emptying times predicted by the DEM and TFM frameworks. Despite this, the overall CPU time required by the MPIC framework simulations was still significantly shorter than the DEM simulations.

Figure 3.15 also highlights the discrepancy in the initial solids fraction of the load, which is better detailed by the results in Table 3.13. This result is likely due to the assumptions made by the MFiX developers when building the solids generation functions in each of the frameworks. The TFM and MPIC cases were able to initialize a solids configuration that agreed quite well with the initial mass load used in the experiments, while the DEM framework initialized a particle bed that was not fully settled and therefore was initially lower in mass than the others.

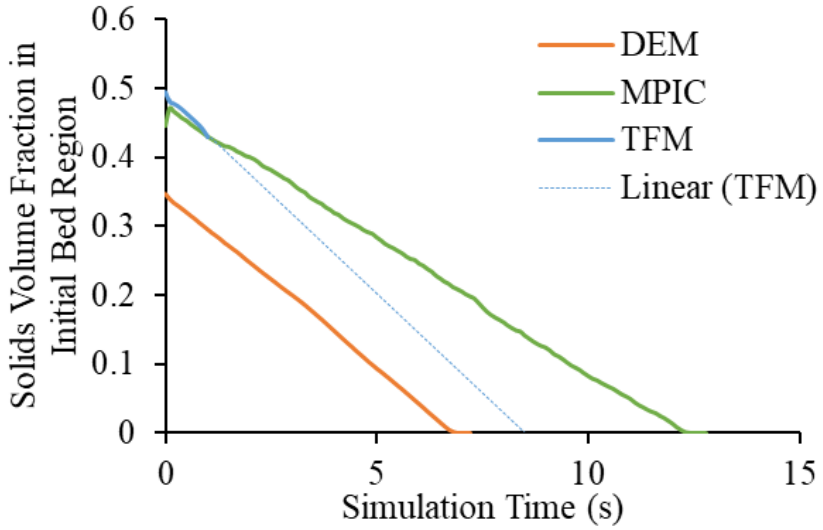

(a)

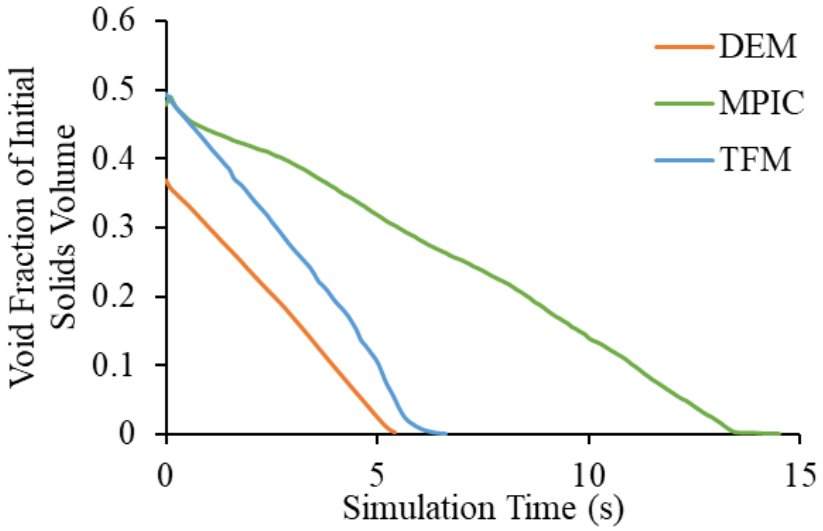

(b)

Figure 3.15. Simulation results for discharge dynamics as predicted by each framework for: **a)** larger particle type #1 cases, and **b)** smaller particle type #2 cases

Table 3.13. Resulting solids initialization fraction and initial solids mass in each of the hopper model cases

Case		Actual Initialized Solids Fraction	Initial Mass (g)
Larger Particles (Type #1)	**DEM**	0.35	656
	MPIC	0.45	844
	TFM	0.49	936
Smaller Particles (Type #2)	**DEM**	0.37	699
	MPIC	0.48	905
	TFM	0.49	936
Experimental		0.53 (estimated)	1000

To normalize the initial solids fraction discrepancy between the cases in the different frameworks, the absolute discharge rate was calculated for each case. This result is presented in Table 3.14. This metric provides a more direct comparison between the frameworks, and shows that the TFM framework proved to be quite capable of capturing pure granular flow dynamics in 3D that agree very well with the more highly resolved DEM framework predictions. The MPIC framework however, still lacked in ability to accurately represent particle collision effects in solids dense flow regimes.

Table 3.14. Absolute rate of mass discharge from each hopper simulation case

Case		Discharge Rate (g/s)
Larger Particles (Type #1)	**DEM**	92.3
	MPIC	66.5
	TFM	110.1
Smaller Particles (Type #2)	**DEM**	139.7
	MPIC	62.8
	TFM	141.8

3.5 Conclusions

Initial selection of an appropriate multiphase modeling framework that satisfies the level of detail, and computational cost restraints of the problem at hand is crucial to the successful use of CFD tools in industry. Simulation predictions from both the 2D fluidized bed and 3D hopper studies differed between all three frameworks, exemplifying the fundamental differences between the modeling methodology approaches employed in each framework for resolving collision effects. In general, the DEM framework gave the most reasonable and accurate predictions for dynamic pressure profile results in the fluidized bed study, and discharge rates in the hopper study. The DEM framework also required the most computational effort in terms of CPU hours compared to the other two frameworks in every single case. In both studies, the TFM framework produced simulation results that compared generally quite well to those from the DEM framework. The MPIC framework resulted in the fastest solve times in all instances, but the TFM framework still required significantly less computational effort than the DEM framework. While in terms of computational

speed/effort/efficiency the MPIC framework outshined the others, it gravely lacked validity and accuracy in simulation predictions of physical aspects of the solids dense multiphase flows studied.

In the context of computational performance, the PETSc linear solver option in the fluidized bed study proved to be more robust than the native pressure solver in all three frameworks by facilitating the use of larger time-steps in the simulations/reducing the number of necessary time steps, however this did not reduce the overall solve time in either the TFM or MPIC framework cases. The most novel conclusion that can be drawn from the fluidized bed study was that the number of necessary time steps was significantly reduced by the PETSc solver in the DEM framework which was influential enough to result in more favorable solve times in terms of CPU effort in the DEM framework by 4-20%. However, the use of larger time-steps when using the PETSc linear solver did reduce the accuracy of simulation predictions for average bed pressure drop in the DEM framework compared to the native solver predictions and the experimental measurements and needs to be explored further.

Another important conclusion from the fluidized bed study was that the MPIC framework appeared to be equally burdened by the pressure solve bottleneck as the TFM framework. The pressure solve bottleneck proved be more of a significant problem in flow regimes of higher solids densities. This was observed in the low velocity fluidized bed case in both of the TFM and MPIC frameworks, and in the troubles converging the TFM framework hopper discharge simulations.

REFERENCES (CHAPTER 3)

[1] Bakshi A, Shahnam M, Gel A, Li T, Altantzis C, Rogers W, et al. Comprehensive multivariate sensitivity analysis of CFD-DEM simulations: Critical model parameters and their impact on fluidization hydrodynamics. Powder Technology 2018;338:519–37. https://doi.org/10.1016/j.powtec.2018.06.049.

[2] Liu P, Hrenya CM. Challenges of DEM: I. Competing bottlenecks in parallelization of gas–solid flows. Powder Technology 2014;264:620–6. https://doi.org/10.1016/j.powtec.2014.04.095.

[3] Li F, Song F, Benyahia S, Wang W, Li J. MP-PIC simulation of CFB riser with EMMS-based drag model. Chemical Engineering Science 2012;82:104–13. https://doi.org/10.1016/j.ces.2012.07.020.

[4] Clarke LE, Krishnamoorthy G. Pre-conditioning strategies to accelerate the convergence of iterative methods in multiphase flow simulations. Mathematics and Computers in Simulation 2019;165:200–22. https://doi.org/10.1016/j.matcom.2019.03.009.

[5] Moliner C, Marchelli F, Bosio B, Arato E. Modelling of Spouted and Spout-Fluid Beds: Key for Their Successful Scale Up. Energies 2017;10:1729. https://doi.org/10.3390/en10111729.

[6] Balay S, Abhyankar S, Adams M, Brown J, Brune P, Buschelman K. {PETS}c Users Manual}. Argonne National Laboratory; 2017.

[7] Clarke L. Interfacing The CFD Code MFiX With The PETSc Linear Solver Library To Achieve Reduced Computation Times. University of North Dakota, 2018.

[8] Vepsäläinen A, Shah S, Ritvanen J, Hyppänen T. Interphase mass transfer coefficient in fluidized bed combustion by Eulerian CFD modeling. Chemical Engineering Science 2014;106:30–8. https://doi.org/10.1016/j.ces.2013.11.042.

[9] Nikolopoulos A, Stroh A, Zeneli M, Alobaid F, Nikolopoulos N, Ströhle J, et al. Numerical investigation and comparison of coarse grain CFD – DEM and TFM in the case of a 1 MW th fluidized bed carbonator simulation. Chemical Engineering Science 2017;163:189–205. https://doi.org/10.1016/j.ces.2017.01.052.

[10] Gopalan B. Small Scale Challenge Problem I. NETL Multiphase Flow Science Team; 2013.

[11] Chen S, Adepu M, Emady H, Jiao Y, Gel A. Enhancing the physical modeling capability of open-source MFIX-DEM software for handling particle size polydispersity: Implementation and validation. Powder Technology 2017;317:117–25. https://doi.org/10.1016/j.powtec.2017.04.055.

[12] Gopalan B, Jonathan T. Dynamic Particle Property Measurement for SSCP-I n.d.

[13] Gopalan B, Shahnam M, Panday R, Tucker J, Shaffer F, Shadle L, et al. Measurements of pressure drop and particle velocity in a pseudo 2-D rectangular bed with Geldart Group D particles. Powder Technology 2016;291:299–310. https://doi.org/10.1016/j.powtec.2015.12.040.

[14] Ketterhagen WR, Curtis JS, Wassgren CR, Kong A, Narayan PJ, Hancock BC. Granular segregation in discharging cylindrical hoppers: A discrete element and experimental study. Chemical Engineering Science 2007;62:6423–39. https://doi.org/10.1016/j.ces.2007.07.052.

[15] Garg R, Galvin J, Li T, Pannala S. Documentation of open-source MFIX–DEM software for gas-solids flows n.d.:40.

[16] Garg R, Garg R, Energy U, Dietiker JF, Dietiker J. Documentation of open-source MFIX–PIC software for gas-solids flows n.d.:20.

[17] Syamlal M, Rogers W, O`Brien TJ. MFIX documentation theory guide. 1993. https://doi.org/10.2172/10145548.

[18] Lungu M, Wang H, Wang J, Yang Y, Chen F. Two-Fluid Model Simulations of the National Energy Technology Laboratory Bubbling Fluidized Bed Challenge Problem. Ind Eng Chem Res 2016;55:5063–77. https://doi.org/10.1021/acs.iecr.5b04511.

[19] Agrawal V, Shinde Y, Shah MT, Utikar RP, Pareek VK, Joshi JB. Effect of drag models on CFD–DEM predictions of bubbling fluidized beds with Geldart D particles. Advanced Powder Technology 2018;29:2658–69. https://doi.org/10.1016/j.apt.2018.07.014.

[20] Syamlal M, O'Brien TJ. The Derivation of a Drag Coefficient Formula from Velocity Voidage Correlations n.d.:20.

[21] Musser J, Fullmer WD, Clarke MA, Dietiker J-F, Weber J, Shahnam M, et al. Comments on mean bed pressure drop in SSCP-I n.d.:3.

CHAPTER 4

Dilute Multiphase Flows: Assessing the Importance of Adequate Characterization of the Particle Size Distribution and the Near-Boundary Spatial Resolution in Modeling Ash Deposition on Heat Transfer Surfaces

Abstract:

In solid fuel combustion systems, ash formation and its deposition on heat transfer surfaces (i.e. boiler tubes) occurs via complex physio-chemical processes that negatively affect boiler operation. The present work demonstrates that significant knowledge gaps still exist in our understanding of ash deposition processes and the need for experimentalists and CFD modelers to work closely together to address these challenges. During combustion, the particle size distribution (PSD) and compositions of the combusting particle/ash evolve as it transitions through the system, but current state-of-the-art Lagrangian combustion modeling methods use a simple "shrinking core" model which does not reflect changes in the PSD observed from additional physical phenomena like fragmentation and coagulation. In lieu of this shortcoming, this work aims to: 1) explore prediction sensitivities to the resolution (bins) of the PSD model, 2) assess the near-boundary spatial resolution requirements to adequately characterize particle impaction and 3) determine and assess a Weber number based formulation for a particle capture sub model by comparing simulation predictions to well

characterized experimental measurements of ash deposit growth rates. This is accomplished by simulating the combustion conditions of three coals (PRB, Illinois and Sufco 2) in a pilot-scale combustor. Adequacy of combustion modeling methodologies was first established by obtaining satisfactory agreement in all three coal cases with experimental measurements of gas temperatures along the axial profile, and ash fluxes at the combustor outlet as well as predicted velocity profiles along the flow direction. These simulation predictions were nearly identical when using both a coarse mesh and a fine mesh, however significant variations in the ash impaction rates (predicted using add-on functions) were observed between the two mesh resolutions across all three coal types. Further, a moderate sensitivity of the ash impaction rates to the number bins employed to resolve the coal PSD was also observed in both meshes. Using the results from the coarse mesh simulations, Weber number based capture criterion were deduced for each coal type by altering the capture criteria to achieve capture efficiencies which gave yield to simulation predictions for ash deposition rates that matched experimental measurements. The Weber number capture criterion values were significantly less than unity and varied across the coals, highlighting the importance of considering of sticking effects and the dangers of using this capture method universally.

4.1 Introduction

Scientists and engineers often deal with dilute dispersed multiphase flows in many different industrial operations where small concentrations of particulate matter are entrained in large fluid volumes equating to solids volume fractions less than 1%. CFD modeling tools

have been employed to help increase understanding of the behaviors and implications of these dilute particulate matter multiphase flows in order to better equip engineers to control them. In the work presented in this chapter, ANSYS Fluent, a powerful commercial CFD software, was used to study the flow of ash particles in flue gas resulting from the combustion of coal with air in an experimental pilot-scale reactor at the University of Utah that was previously designed to emulate a coal-fired steam boiler. The aim of this work was in the direction of developing a sub model capable of predicting the growth rates (mass accumulation) of ash deposits on a heat transfer surface (i.e. a boiler tube).

In the energy industry, the combustion of solid fuels in a boiler has long been a common mode of producing intense heat to efficiently vaporize water into steam for electric power generation. Efforts to retain coal-fired power plants while meeting targets to reduce fixed carbon emissions has led to an increase in CFD modeling and simulation research to facilitate investigations into the complex environment of traditional coal combustion systems, as well as emerging new technologies such as oxy-fuel combustion, and/or new fuels like biomass.

Of specific concern in this chapter is the growth rates of outer ash deposits on the combustion gas side of boiler tubes where energy released during combustion is transferred to a working fluid (in most cases boiler feedwater) in order to vaporize the fluid for energy extraction or utilization elsewhere. Ash deposition on heat transfer surfaces can negatively impact boiler operations by reducing the radiative heat transfer effects (i.e. emissivity and absorptivity) due to the naturally occurring mineral content in ash [1]. Ash deposition can

also decrease the conductive heat transfer as these minerals have much lower thermal conductivities compared to the metals of the bare tubes [2]. These impacts in turn can reduce the overall heat transfer efficiency between the combustion gases and the working fluid. Ash deposition in boilers can also lead to other common slagging and fouling problems like under-deposit corrosion and increased downtime for cleaning [3]. Accounting for all the complexities of the physio-chemical processes involved in ash deposition is quite challenging, and requires the creative evolution of numerical and computational modeling methodologies beyond those already previously rigorously developed for simulating coal combustion.

4.1.1 Challenges in Modeling Coal Combustion

Naturally, the merit of any successful ash deposition modeling effort relies on the methodologies used to model the combustion process itself. In brief, combustion is understood by researchers as an aggregate network of highly intricate physical and chemical processes. Combustion is controlled by both homogenous and heterogenous physical and chemical processes like pyrolysis, oxidation, vaporization, devolatilization, and char burnout [4]. These processes are driven by other phenomena including diffusion of species (fuels, oxidizers, and products) and reactions of these species (coal with oxidizers by pyrolysis, and pyrolysis products with gaseous oxidizers) [4]. In combustion modeling efforts that are concerned with ash deposition such as in this work, another important combustion process/phenomena to capture is ash formation which occurs by several other underlying

combustion processes including nucleation, coagulation, agglomeration, condensation, and particle shedding and fragmentation. These processes have been experimentally observed to alter both char and ash particle characteristics, including particle size [5–7]. Some CFD researchers have previously attempted to model coagulation and fragmentation effects to simulate ash formation, while others assumed that these effects are negligible and ignored them. In both cases acceptable combustion simulation prediction accuracies have been achieved [8,9].

The field of CFD combustion modeling is rich in abundance of approaches, both Lagrangian and Eulerian, to capture the nature and nuances of solid fuel combustion. In previous work conducted by UND ChE graduate student Trevor Seidel [9,10], two frameworks available in ANSYS Fluent were studied to test the capability of appropriately characterizing combustion conditions observed in physical experiments on a pilot-scale oxy-fuel combustor (OFC) from previous research by the University of Utah. The two ANSYS Fluent frameworks investigated (in axisymmetric 2D) were the Two Fluid Model (TFM) and the Discrete Phase Model (DPM). In the Fluent TFM framework, the particle phase, which includes both coal and ash particles, is represented as a continuous interpenetrating phase along with the fluid phase which consists of the oxidizer and combustion (flue) gases. The Fluent TFM framework is governed by Euler-Euler equations like those detailed previously in section 2.3 of this thesis. In the Fluent DPM framework, the fluid phase is still treated as a continuum, but the particle phase is resolved as a distribution of characteristic particles of varying frequency, each representing a range of real particle diameters. The Fluent DPM

framework is a hybrid multiphase model which computes interphase transfers in the Eulerian grid, but maintains Lagrangian frame tracking of particles which can be a valuable tool when studying ash deposition. One common particle size distribution model supported by ANSYS Fluent DPM is the Rossin-Rammler curve which can be fitted to a desired PSD assuming an exponential relationship exists between a particle diameter and the mass fraction of particles with a greater diameter [11,12].

As far as predicting flame stability and ignition behaviors, both the TFM and DPM frameworks, equipped with equally valid CFD coal combustion functions/sub models, were able to reasonably predict OFC reactor profiles of temperature and velocity in 2D axisymmetric simulations [10]. The DPM framework produced only marginally better results in swirling flame scenarios than the TFM framework [10]. The modeling parameters and additional user-defined functions used in both cases were also capable of adequately considering complex radiative heat transfer effects of coal combustion observed in the University of Utah experiments [10]. It was also demonstrated that the DPM framework was more capable than the TFM framework for predicting realistic particle dispersion in swirling flame combustion simulations which is inherently important to capture in studying ash deposition [10].

In the context of ash formation during combustion, the TFM framework is more equipped than the DPM framework to handle changing particle size distributions with coagulation and fragmentation sub models. However as the complexity of TFM combustion models increases with the need to solve more and more extensive sub models for particle

polydispersity, these simulations become increasingly unstable and difficult to converge [13]. To maintain an appreciative computational cost advantage over the DPM framework, combustion models in the TFM framework require gross assumptions to be made about the distribution of particle sizes such as uniform diameter of the pulverized coal particles. This reinforces the observations from Seidel [10] that the TFM framework struggled to accurately characterize particle dispersion in swirling combustion scenarios.

In modeling both combustion and ash deposition, one of the biggest challenges facing hybrid Lagrangian models, like ANSYS Fluent DPM, is appropriate characterization of the particle size distribution. Some attempts have been made to measure the particle size distributions experimentally throughout the entirety of a boiler, but many CFD studies do not apply adequate resolution to the PSDs [14]. Previous work from Krishnamoorthy and Wolf [1] suggests that at least 40 bins in a Rossin-Rammler PSD model are needed to capture appropriate particle radiative properties and effects throughout the boiler, when commonly only 10-20 are employed in most CFD studies.

4.1.2 Challenges in Modeling Ash Deposition

Research concerning the umbrella issue of ash deposition can be divided into separate generalized efforts focused on: ash particle formation, fluid dynamics (particle transport and boiler design), ash deposit formation and deposit growth on heat transfer surfaces, the material properties of ash deposits themselves, and the effect of ash deposits on heat transfer efficiency [15]. Traditional slagging and fouling indices along with soot blowing routines

have helped minimize the negative impacts of ash deposition in combustion operations, but still much understanding is left to be desired. Briefly summarized below is a list of potential sub models (some theoretical, some empirical) and their inputs/important variables that would be required to completely consider the numerous physical and chemical phenomena observed in the combustion and ash deposition process [15]:

i. Combustion codes
   - evaporation, oxidation, pyrolysis
     - fuel analyses, ash analyses, power plant design, operating conditions
     - homogenous and heterogenous reaction rates

ii. Ash formation
   - coalescence, vaporization, homogenous nucleation
   - heterogenous condensation, fusion, fragmentation, expansion
     - ash analyses
     - inherent mineral compound compositions
     - allocation between included and excluded particulate matter within the solid fuel plus those that are organically bound in the carbon matrix

iii. Ash particle transport
   - inertial and thermophoresis kinetic/diffusion mechanisms
     - particle size, particle temperature

iv. Ash particle impaction
   - dynamic kinetic models

v. Ash particle sticking
   - viscosity based or melt fraction
     - particle and deposit viscosities, softening temperature

vi. Ash particle rebound
   - energy and/or force balance

- incident angle, restitution coefficients

vii. Ash particle removal

- energy balance, energy dissipation, critical moment
- force and momentum balance
  - internal energies, enthalpies

While a model this detailed would be very well suited to provide great insight to predicting ash deposition rates and effects in a boiler, it is easier said than done, and is likely not applicable across all fuel types with a single collection of inputs, nor would it be at all desirable in terms of computational costs.

Ash deposition on a heat transfer surfaces, commonly reported in units of mass flux, is governed by several key mechanisms including inertial impaction, thermophoresis, condensation, surface reactions, and turbulent eddy deposition either from within or outside the boundary layer [15]. Previous experiments have shown that the most dominant mechanisms for ash transport and deposition on coal-fired boiler tubes are inertial impaction and thermophoresis [16]. Inertial impaction is the most dominant because it affects mostly larger ash particles (> 10 microns) and depends on the local flow regime, the target geometry, the particle size, and the particle density. Thermophoresis also contributes significantly to ash deposition, affecting mainly medium sized particles due to the temperature gradient between the ash particle and the surface. Thermophoresis depends primarily on individual particle and local surface temperatures.

Recognizing that these mechanisms play the most important roles in ash deposition, the following functional relationship can be derived which helped guide the work presented in this chapter:

$$\eta_o = \frac{r_{deposition}}{\dot{f}_f * w_{ash}/A_c} = q_p * \eta_i * \eta_c \qquad \textbf{Eq. 4.1}$$

Where η_o refers to the overall collection efficiency, $r_{deposition}$ is the rate of ash deposition, $\dot{f}_f$ is the flowrate of fuel or pulverized coal with ash content weight fraction of w_{ash}, A_c is the cross-sectional area of the combustion reactor, q_p is the total particle flux, η_i refers to impaction efficiency, and η_c refers to capture efficiency.

The right hand side of Equation 4.1 considers what fraction of particles flowing past a heat transfer surface is likely to impact the target, and what fraction of the particles which impact the heat transfer surface are likely to actually adhere or stick and deposit.

Impaction rates, or the rate that particles come into contact with a surface of interest as a result of flow over/around an obstacle, has previously been researched and modeled with quite surprising accuracy by others [15,17,18]. According to Weber et al [19], [19], the thickness of the boundary layer (layer of fluid flow nearest the surface with thickness determined by local flow regimes) should contain at least four computational nodes/volumes in order to adequately predict particle impaction rates during flow over a cylinder. In a pilot scale study this near-boundary spatial resolution can be reasonably obtained as it is in the present work, but can become almost impossible to realistically manage in simulations of

industrial sized boilers with hundreds of heat exchanger tubes and complex flue gas recycle/venting systems.

In lieu of the challenges discussed, one objective of this work was to attempt to simulate impaction rates of ash particles on a cylindrical geometry protruding into the radiative exhaust zone of a combustor (representing the collection probe used in experiments to emulate boiler tubes) as appropriately as possible with established CFD modeling methodologies for combustion. Further, another objective was to study the sensitivity of impaction rate predictions to the mesh resolution and the resolution of the particle size distribution model.

In this work, capture rates/capture efficiency represents the propensity of a particle to deposit on a surface. This physical phenomenon is heavily influenced by multiple variables including the kinetic energy of the particle during impaction, and the viscosity and surface tension of both the particle and the surface during impaction. Consequently, appropriate modeling of the capture process requires adequately resolving the PSD model and the spatial resolution near the surface as well. The aim of the modeling and simulation work presented in this chapter is in pursuit of formulating a particle capture (and removal) add-on function/sub model with the ability to directly estimate impaction rates from combustion simulation results and to further calculate capture efficiencies required to ultimately predict deposition rates. This was attempted by determining capture efficiencies necessary to predict ash deposition rates of multiple coal types which agreed with experimental measurements.

One simplified approach for formulating particle capture, initially identified for potential in CFD modeling by Weber et al. [20], is similar to traditional critical viscosity or critical temperature predictive methods, but relies less on arbitrary critical values from literature, and focuses more on fuel-dependent properties like ash analyses. The critical Weber number capture method is rooted in the assumption that inertial impaction can be adequately accounted for by rigorous CFD modeling methodologies of the combustion process. Then, a Weber number can be calculated for each individual impacting particle and compared to a critical value to decide if the particle sticks or not. The Weber number describes the ratio of the kinetic energy of a particle passing over a surface to surface tension forces, and is calculated by many of the variables which are important to the main mechanisms of ash deposition. Particle Weber numbers in this work are calculated as follows:

$$We = \frac{\rho_p * d_p * {v_p}^2}{\sigma} \qquad \textbf{Eq. 4.2}$$

Where $\rho_p$is the particle density, d_p is the particle diameter, v_p is the particle velocity magnitude, and σ is surface tension.

Surface tension is a function of the chemical composition of the ash, and can be calculated by an empirical model given by:

$$\sigma\ (N/m) = \sum(0.001\bar{\sigma_i}\, x_i)\ - 0.00015(T_p - 1733) \qquad \textbf{Eq. 4.3}$$

Where x_i is the mass fraction of mineral component i, and T_p is the particle temperature.

Coefficients for partial surface tension terms ($\overline{\sigma_i}$) used in the calculations in this work were determined by Yong [21], and ash analyses necessary for this calculation are presented later.

A simple expectation which is commonly believed in literature, would be that ash particles near a surface with a Weber number less than unity (1) would stick, while those with a greater Weber number would either rebound or remain entrained in the fluid phase and pass over the target surface. Calculating/identifying a critical Weber number that satisfies this situation to yield comparable deposition rates to those measure experimentally for multiple different coal types was a resulting outcome of the work presented in this chapter.

4.2 Description of U of Utah Ash Deposition Experiments

A wealth of experimental data on ash deposition rates from both air and oxy combustion of various solid fuels, including different types of coal and natural gas/biomass blends, was made available by the University of Utah's Department of Chemical Engineering and Institute for Clean and Secure Energy [22]. They conducted combustion experiments on 35 different fuel blends and oxidizer condition combinations and measured the growth rates of both inner and outer ash deposits.

Three sets of conditions from coal/air combustion experiments were selected to be modeled and analyzed based on their diversity. The selected coal types were:

- Powder River Basin (PRB), subbituminous coal with low ash content which produced smaller ash deposit growth rates
- Illinois #6, a bituminous coal with high ash content producing moderate ash deposit growth rates
- Sufco 2, a bituminous coal with low to moderate ash content but was observed to produce larger ash deposit growth rates

The published experimental ash deposition rates this work aims to predict and their corresponding overall collection efficiencies are reported in Table 4.1.

Table 4.1. Results for outer ash deposit growth rates and overall collection efficiencies reported for select trials from University of Utah's combustion experiments [22]

Fuel	**Measured outside ash deposit growth rate (g/m^2h)**	**Reported overall ash collection efficiency (wt %)**
Powder River Basin (PRB) (sub-bituminous coal)	53.7 ± 1.00	1.34%
Illinois (bituminous coal)	124.04 ± 1.00	2.06%
Sufco 2 (Utah bituminous coal)	338.77 ± 59.80	3.92%

The measured ash deposition rates were gathered from experiments conducted on the University of Utah's 100kW (rated) down-fired oxy-fuel combustor (OFC) pictured as a schematic in Figure 4.1. The self-sustained and controlled pilot scale combustor was operated at a firing rate of 27kW, with realistic air to fuel ratios (~3% exhaust O_2 by dry volume). The

combustor exhibited turbulent diffusion flames in the ignition zone, as well as laminar exhaust flow, with realistic industrial boiler residence times. Boiler tube heat transfer surfaces were emulated using an ash collection coupon probe in the exhaust zone around port 6 that was temperature controlled (with air) to 922K.

The experimenters at the University of Utah also measured the gas temperature at the center of the OFC at various points along the axial direction and also reported estimates of gas velocities along the reactor as well. This data was used as metrics for validating combustion simulation predictions.

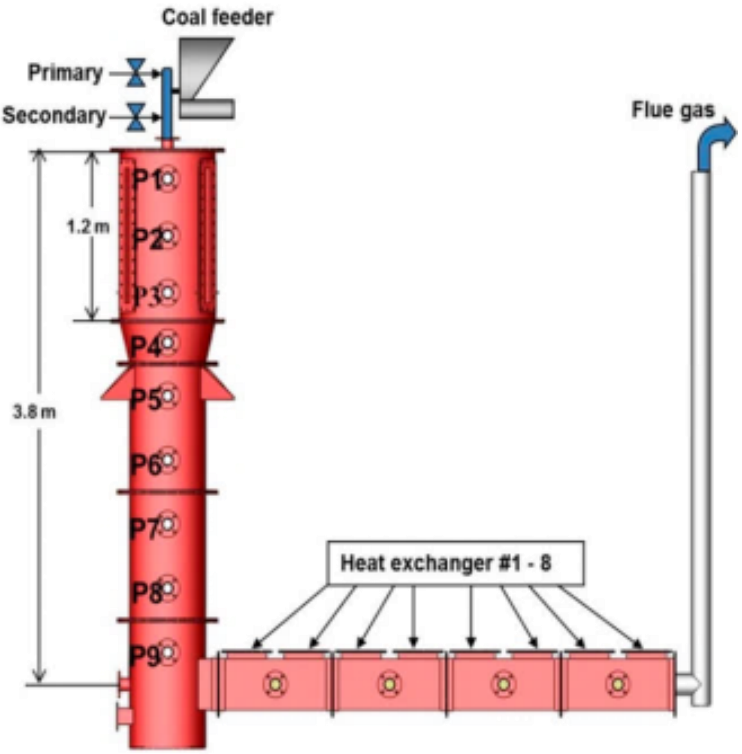

Figure 4.1. Schematic of University of Utah's experimental oxy-fuel combustor (OFC) [22]

4.3 Modeling Methodologies

This work utilized the Discrete Particle Method (DPM) commercial CFD framework in ANSYS Fluent 19.2 to simulate 3D steady state combustion scenarios modeled after the physical OFC experiments from the University of Utah. The three main case scenarios include the combustion of PRB coal with air (PRB_AIR), Illinois coal with air (ILLINOIS_AIR), and Sufco 2 coal with air (SUFCO2_AIR). Figure 4.2 illustrates the geometry built in ANSYS Workbench to model the University of Utah reactor. The total geometry length is 3.8 meters and is comprised of three main zones. The ignition zone is 1.2 meters in length with a diameter of 0.6 meters, and the radiation zone is 2.3 meters in length with a diameter of 0.25 meters. The converging zone merges the ignition zone diameter into the radiation zone diameter over a length of 0.3 meters to diminish the swirling behavior seen in the ignition zone as a desired effect of the coaxial burner design which is also reflected in the model geometry. At 2.3 meters away from the burners, a cylindrical geometry was created with a length of 0.135 meters and a diameter of 0.06 meters to model the ash probe used in the University of Utah experimental facility. Two different meshes were used in this work: coarse (~120K cells) and fine (~1,100K cells). In the fine mesh case, the resolution in the boundary layer was on the order of 10^{-4} m.

The reactor wall boundaries were each set to thermal boundary conditions deemed adequate in previous modeling efforts of the same experiments [10]. The wall temperature of the ignition zone was set at 1250K, the radiation and converging zone walls were set as

convective boundaries with a heat transfer coefficient of 5 W/m^2K and a free stream temperature of 300K. The ash probe boundary was set at a temperature of 922K to model the temperature controlled (air) probe used in the experiments. The reactor exhaust was set as a pressure outflow boundary operating at atmospheric pressure. Table 4.2 outlines the conditions of the inlet streams at the burner entrance for each case that were used to model the different experimental trials. The primary burner consists of mainly pulverized coal with balance of air, and the secondary burner provides the bulk air stream.

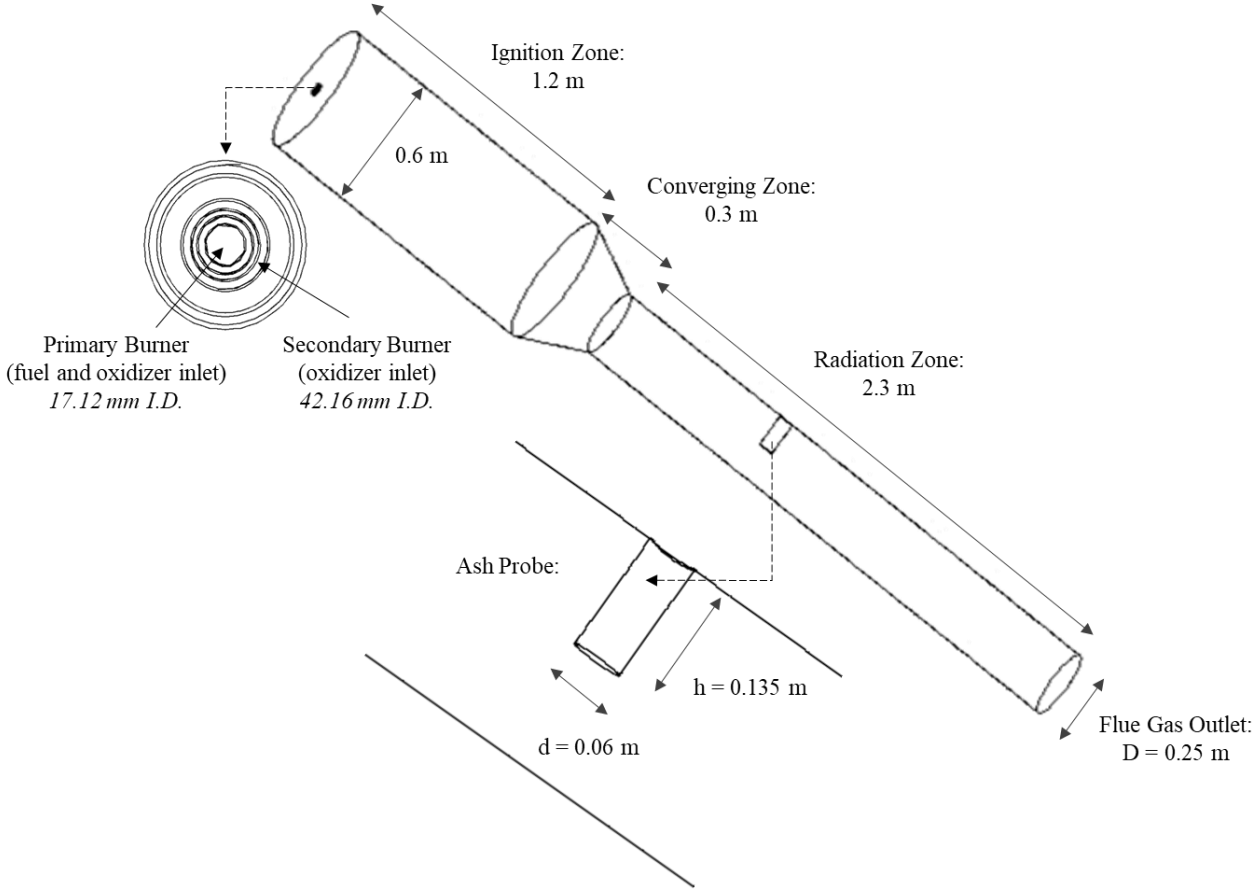

Figure 4.2. 3D geometry designed to model University of Utah's experimental OFC

Table 4.2. Inlet stream boundary condition specifications employed in each case

Inlet Stream Specifications	Cases		
	PRB_AIR	**ILLINOIS_AIR**	**SUFCO2_AIR**
Fuel Mass Flow Rate (kg/h)	4.54	3.56	3.46
Burner Inlet Mass Flow Rates (kg/h)			
Primary (premixed air and fuel)	9.07	9.07	9.07
Secondary (air)	29.62	26.13	24.93
Inlet Gas Temperature of Burner Streams (K)	480	480	480
Gas Species Concentration in Burners (mol%)			
O_2	21	21	21
N_2	79	79	79

The fuel stream in each case was represented by a DPM injection of pulverized coal with unique sieve mass fraction size distributions which were modeled by a Rosin-Rammler curve fit as detailed in Figures 4.3-4.5. Sensitivity of simulation results to the number of bins, or resolution, applied to resolve the initial coal particle size distribution was explored throughout this work.

Each model case was also adjusted to reflect the unique chemical composition of the coal types as measured and reported by the experimenters [22]. Table 4.3 outlines the proximate and ultimate elemental analysis of the PRB, Illinois, and Sufco 2 coals that were being modeled. Additionally, Table 4.4 describes their ash constituents as necessary for calculating surface tension by Equation 4.3.

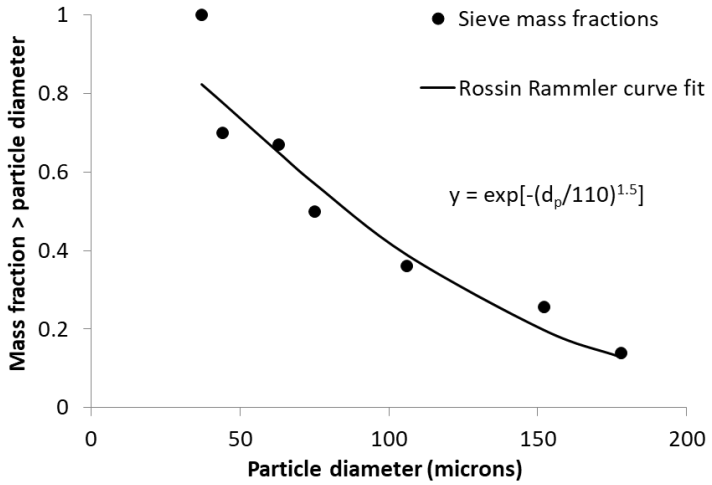

Figure 4.3. PRB coal particle size distribution [4] and Rosin-Rammler curve fit employed to model parent fuel particles in all PRB_AIR cases

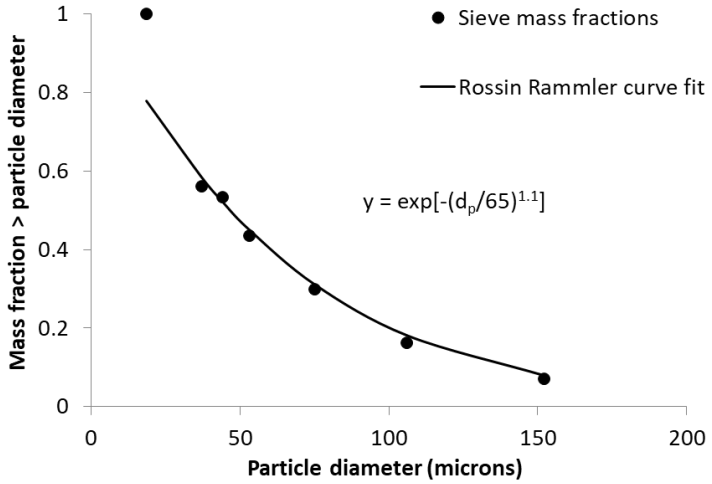

Figure 4.4. Illinois coal particle size distribution [12] and Rosin-Rammler curve fit employed to model parent fuel particles in all ILLINOIS_AIR cases

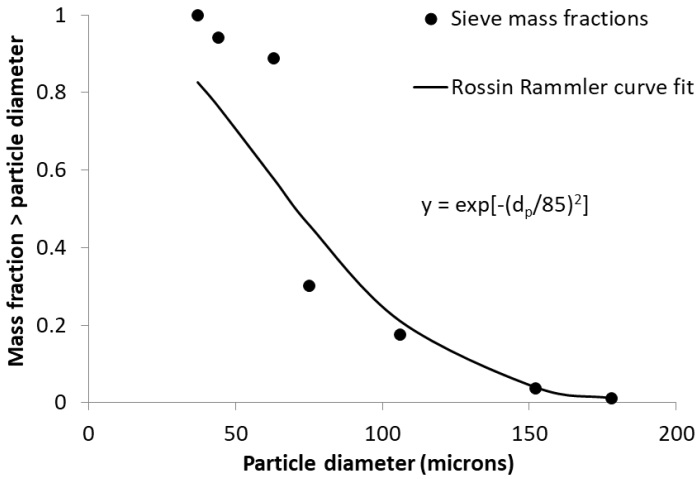

Figure 4.5. Sufco 2 coal particle size distribution [4] and Rosin-Rammler curve fit employed to model parent fuel particles in all SUFCO2_AIR cases

Table 4.3. Proximate and ultimate analysis of the coal types being modeled [22]

Fuel Type	Proximate Analysis (wt%)		Ultimate Analysis (wt%, moisture free basis)	
PRB	*Fixed Carbon*	38.01	*C*	75.27
	Volatiles	33.36	*H*	5.03
	Ash	4.94	*N*	1.09
	Moisture	23.69	*S*	0.32
	HHV (kJ/kg)	21115	*O*	18.29
Illinois	*Fixed Carbon*	44.90	*C*	79.35
	Volatiles	36.04	*H*	5.58
	Ash	9.42	*N*	1.27
	Moisture	9.64	*S*	0.42
	HHV (kJ/kg)	26870	*O*	13.38
Sufco 2	*Fixed Carbon*	42.16	*C*	78.47
	Volatiles	37.36	*H*	5.68
	Ash	13.96	*N*	1.39
	Moisture	6.52	*S*	0.58
	HHV (kJ/kg)	27319	*O*	13.88

Table 4.4. Ash analyses of the selected coal types [22]

Fuel Type	Ash Analysis (wt%)										
	Al_2O_3	CaO	Fe_2O_3	MgO	MnO	P_2O_5	K_2O	SiO_2	Na_2O	SO_3	TiO_2
PRB	14.78	22.19	5.2	5.17	0.01	1.07	0.35	30.46	1.94	8.83	1.3
Illinois #6	20.18	3.22	16.46	0.89	0.03	0.1	2.1	51.22	1.06	2.79	0.98
Sufco 2	12.09	11.9	3.62	3.94	0.03	0.25	1.13	62.48	0.81	1.83	0.68

Generalized combustion reaction mechanisms were employed in all cases which include homogenous and heterogenous reactions that were represented by their kinetic parameters, as provided in Table 4.5. The devolatilization combustion process was modeled with a constant kinetic rate of $50s^{-1}$. This means that the rate at which the volatilized species are released from the coal is independent of the concentration of volatiles. After the volatiles are released, the remaining char particles are oxidized by the surrounding gases.

The gas phase combustion process was modeled as two steps. First, the volatile species are oxidized, which produces CO as seen in Table 4.5. By specifying the coal composition in each case, this reaction is automatically balanced to reflect each unique coal composition. Finally, complete combustion was modeled with the further oxidation of CO to CO_2. A kinetics/diffusion combustion model that uses harmonic averaging of the diffusion and kinetic rates was selected to govern the reaction processes described above. When the particle is large combustion is diffusion limited and when it is small it is kinetic limited.

The realizable k-epsilon turbulence model was employed for all preliminary results in this study. In section 4.4.1, the effect on simulation results to the selection of another more involved turbulence model, the SST k-omega model, is discussed. Additionally, user-defined functions were written to model the solid and fluid phase radiative properties. These models consider the non-grey effects of gas phase radiation and the variations in particle radiative phase properties. These functions were based on previous coal combustion modeling by Krishnamoorthy and Wolf [1].

Table 4.5. Summary of reactions and kinetic parameters employed in all modeling cases of the University of Utah experiments

Reactions	**Pre-exponential Factor, A**	**Activation Energy, Ea (J/kmol)**	**Reference**
Heterogenous reactions:			
Devolatilization	Constant 50 (1/s)		
Char combustion $2C_s+O_2 \rightarrow 2CO$	0.002 (kg/m^{2}sPa)	7.90E+07	[23]
Homogenous reactions:			
Volatile combustion (unbalanced) $vol+O_2 \rightarrow CO+H_2O+N_2+SO_2$	2.119E+11 (1/s)	2.03E+08	[24]
CO complete oxidation $2CO+O_2 \rightarrow CO_2$	2.239E+12 (1/s)	1.70E+08	[25]

Table 4.6. Summary of modeling options evoked to model the University of Utah combustion experiments

Physics Being Modeled	CFD Model (ANSYS Fluent)
Multiphase hydrodynamics	DPM
Turbulence	Realizable k-epsilon
Drag law	Morsi-Alexander
Near wall treatment	Standard wall functions
Coal devolatilization	Constant
Gas phase chemistry	Finite rate/eddy dissipation
Combustion model	Diffusion limited
Heterogenous chemistry	Particle surface reactions
Particle radiative property	Variable K_{abs} and K_{scat} [1]
Particle scattering phase function	Isotropic
Gas phase radiative property	Perry (5gg) [26]

4.4 Results and Discussion

The novelty of this work lies in the investigation of impaction rates and capture efficiencies, but preliminary simulation results were validated against available experimental data [6] to acknowledge appropriate CFD combustion modeling techniques before ash deposition behavior was explored. Outlet/exhaust oxygen concentrations and ash fluxes in the flue gas ascertain confidence in the combustion modeling methodologies employed to capture complete combustion. Additionally, profiles of gas temperatures and velocities were also initially important to achieving adequate representations of particle temperatures and momentum.

4.4.1 Combustion Simulation Validation

Figure 4.6 illustrates oxygen contours of the OFC and provides visual representation of air combustion condition results from the different coals. In the previous University of Utah experimental work [6], the oxidizer supply was controlled to maintain about 3 vol% excess oxygen in the dry exhaust as opposed to maintaining a specific stoichiometric inlet ratio. As seen in the contours below, the predicted oxygen concentrations at the reactor outlet were roughly lower than a mol fraction of 0.03. However, carbon monoxide concentrations at the reactor outlet in the simulations were extremely negligible, around $1x10^{-6}$ mol fraction, indicating the simulations were still achieving complete combustion. Additionally, Table 4.7 compares the predictions for ash fluxes in the exhaust gas with experimental data. At this point, no capture/removal models were being employed, so it is to be expected that the predicted outlet ash concentrations are greater than the measured values and also given the variation in exhaust gas temperatures (to be discussed next), these results were acceptable indications of satisfactory modeling techniques for combustion and ash formation.

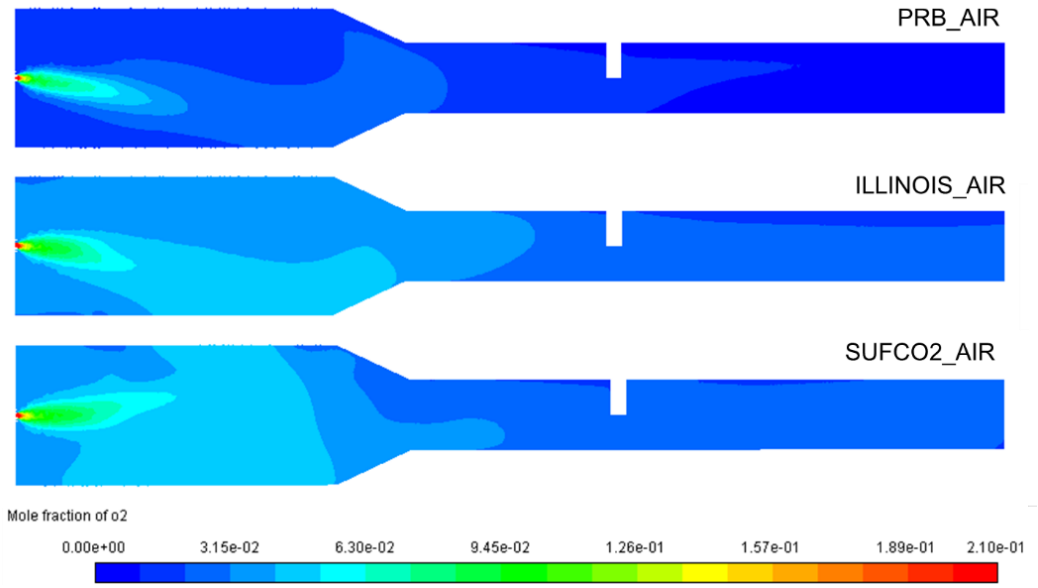

Figure 4.6. Visualization of oxygen concentration (mol fraction) contours from 3D simulations of combustion with air of three different coal types

Table 4.7. Comparison of measured and predicted flue gas ash concentrations

Case	**Ash concentration in flue gas (g/m^3 std)**	
	Measurement	*Simulation*
PRB_AIR	7.26	12.1
ILLINOIS_AIR	11.58	13.6
SUFCO2_AIR	n/a	14.7

Figure 4.7 displays the reactor temperature contours of the OFC for each coal type case and again provides visual representation of the combustion conditions predicted for each coal. Predicted peak temperatures in the ignition zone were unique to each coal type as expected, and were over predicted by less than 10% compared to measurements recorded

[22]. The temperature around the ash probe position, as indicated by the notch in the contour, was also only slightly over predicted compared to the 1100-1200K range recorded by the experimenters at that location [22].

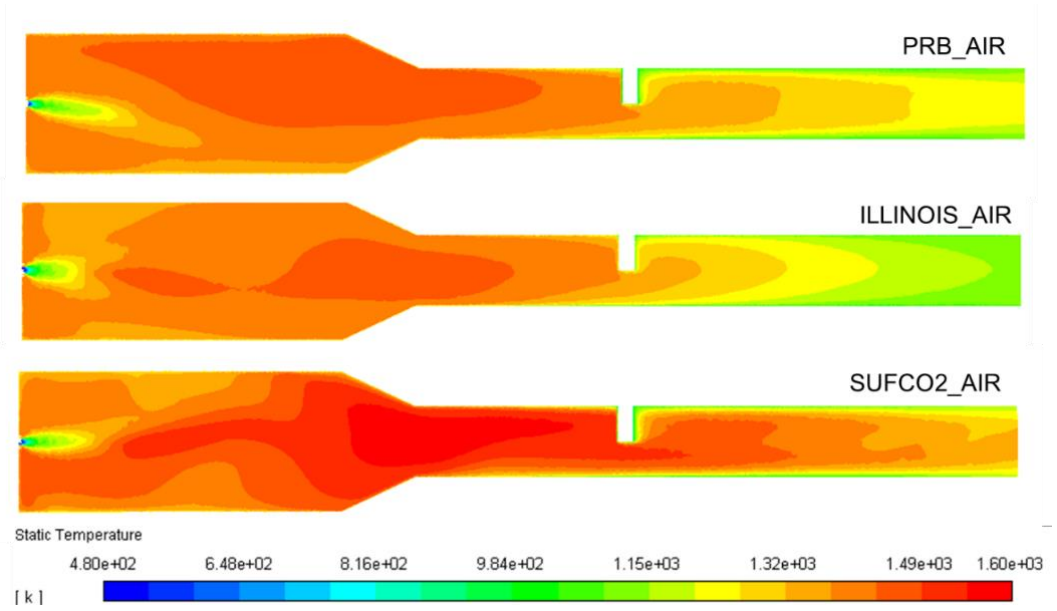

Figure 4.7. Visualization of OFC temperature (K) contour results from 3D simuations of combustion with air of three different coal types

Figure 4.8 shows the axial temperature profiles from each simulation case compared to the experimental measurements. Temperature is more overpredicted in the Sufco 2 case. This is most likely due to overestimating the secondary burner rate when establishing the model boundary conditions, since no experimental information about the exact mass flow rate of air used in the Sufco 2 experimental trials was available as it was for the other two coal trials. However, all simulation predictions for temperature are within a couple hundred degrees of the thermocouple measurements which is considered satisfactory at this stage of modeling efforts.

In addition to temperature, velocity was validated against experimental estimates to evaluate the combustion modeling methodologies before analyzing ash deposition. Figure 4.9 compares the measured gas velocities to simulation predictions in each case in the radiation zone where ash particle behavior is of interest. Velocity profile comparisons in the ignition zone are not of concern, as the swirling behavior results in calculated gas velocity magnitudes that do not make sense to compare against experimental measurements. Results for simulation predictions of gas velocities are overall satisfying, once again confirming acceptable combustion modeling techniques.

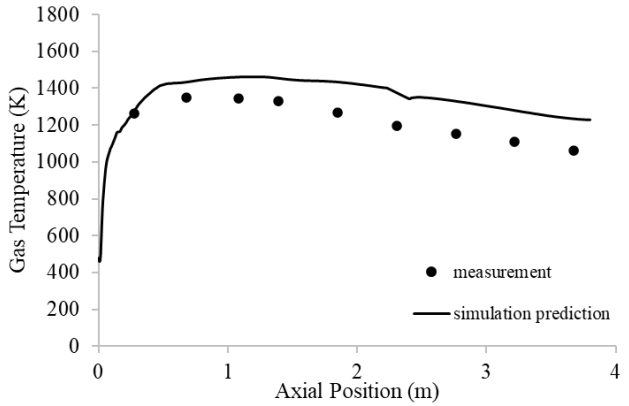

(a)

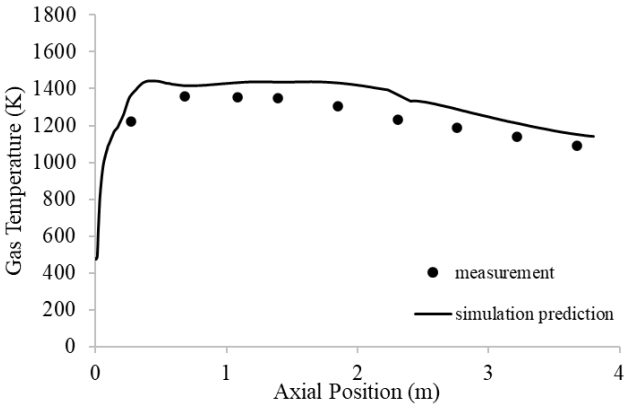

(b)

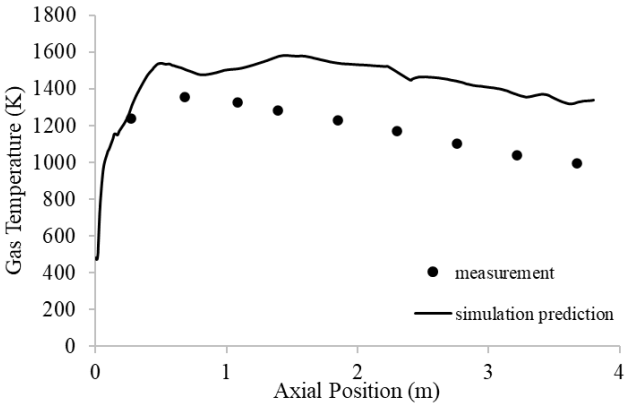

(c)

Figure 4.8. Predicted axial temperature profiles compared to experimental measurements [6] for cases: **a)** PRB_AIR **b)** ILLINOIS_AIR and **c)** SUFCO2_AIR

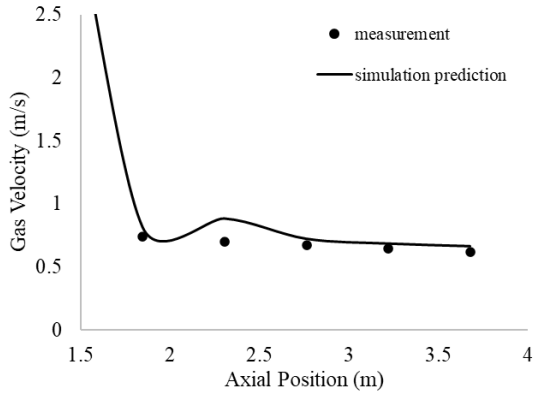

(a)

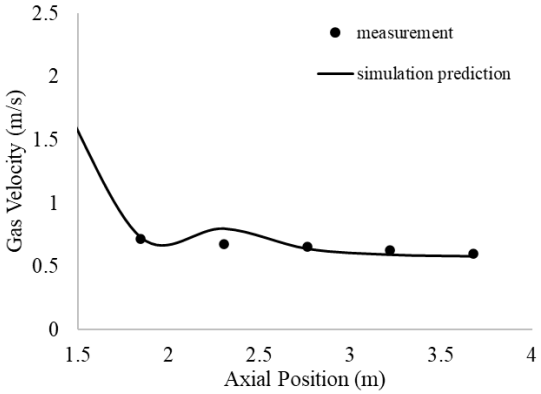

(b)

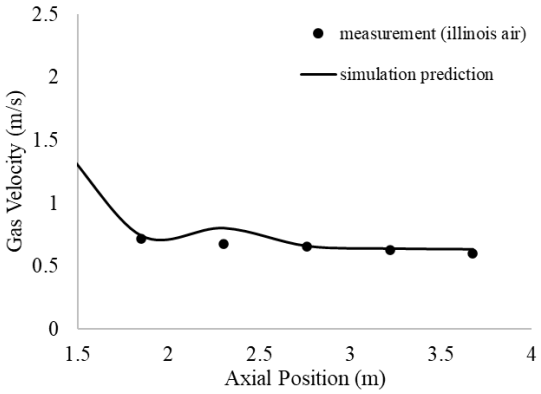

(c)

Figure 4.9. Predicted gas velocities in the radiation zone compared to experimental measurements [6] for cases: **a)** PRB_AIR **b)** ILLINOIS_AIR and **c)** SUFCO2_AIR

Simulation results for predicted temperature and velocity profiles were only mildly improved by certain changes in modeling parameters that are of interest in this work. First, Figure 4.10 shows the effect on these combustion validation results by increasing the resolution, or number of bins, applied in the Rosin-Rammler particle size distribution model. Increasing the number of histogram bins used to resolve the RR model increases the accuracy of the fit to measured particle sizes, but also the computational effort required to converge the simulations. In the Illinois case, the 80 bin RR resolution appeared to improved the simulation prediction for temperature especially at the outlet, but at port 6 where the collection probe is, the predicted temperature was only closer to the experimental measurement by 4%. Considering the inherent degree of variability in the experimental measurements, the variability in simulation results using 20, 40, or 80 RR bins is negligible in the cases of all three coal types.

Figure 4.11 depicts the effect on temperature and velocity profile predictions of using a more refined mesh, and a more enhanced SST k-omega turbulence model. Similar to Figure 4.10, combustion validation results were only mildly improved by these modeling parameters.

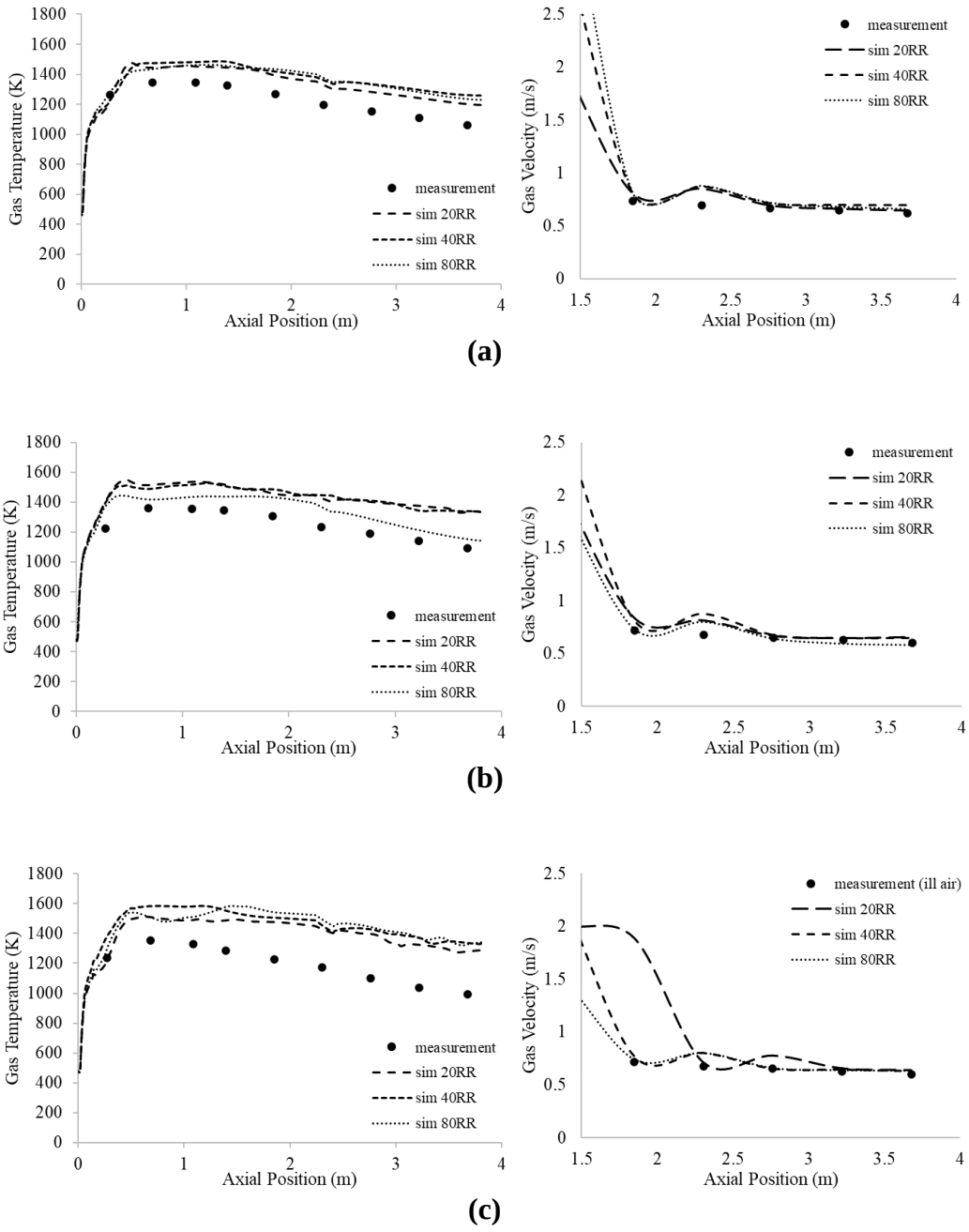

Figure 4.10. Comparison of predicted reactor profiles of axial temperature (left) and velocity (right) with different numbers of bins in the RR PSD model for cases: **a)** PRB_AIR **b)** ILLINOIS_AIR and **c)** SUFCO2_AIR

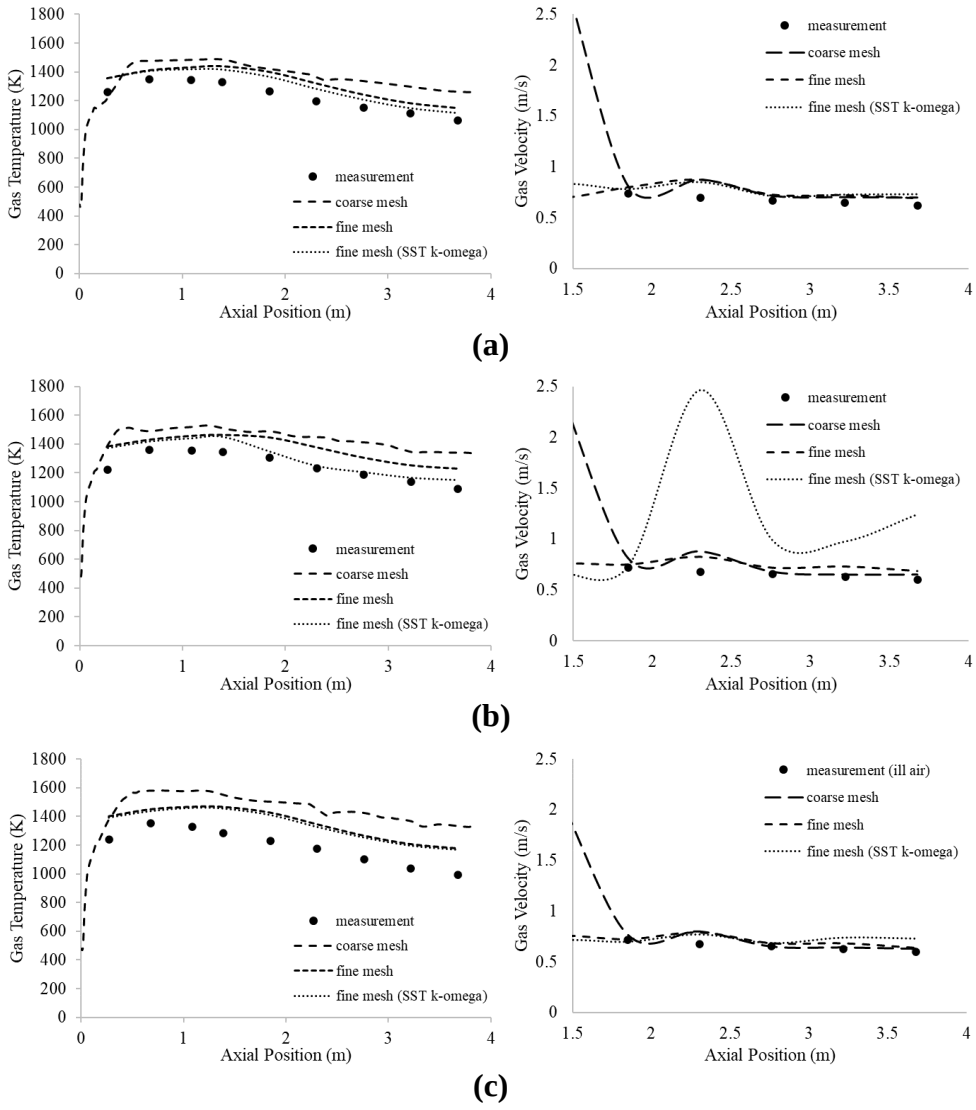

Figure 4.11. Comparison of predicted reactor profiles of axial temperature (left) and velocity (right) with different mesh resolution/turbulence modeling options for cases: **a)** PRB_AIR **b)** ILLINOIS_AIR and **c)** SUFCO2_AIR

4.4.2 Ash Impaction Rates Results

Table 4.8 summarizes the ash impaction rates processed from simulation results using 40 RR bins and the coarse spatial mesh resolution. These values were obtained assuming that all the particles contained within the mesh cell nearest the probe boundary are all considered to be impacting the probe. At this point, no capture or removal models were being used, so these values are indicative of impaction rates, or ash deposition rates assuming 100% capture. The predicted impaction rates were much larger than the measured values for deposit growths. This suggests that impaction rates alone are not enough to predict ash deposit growth rates with the modeling methodologies used, and that a capture/sticking model which adjusts the impaction rate by a capture efficiency is necessary for accurate predictions of ash deposition rates. Table 4.8 also lists the capture efficiency that would be required by a capture/collection sub model to result in accurate simulation predictions for ash deposit growth rates that compare to those measured in the University of Utah experiments. The capture efficiencies calculated appeared to be unique to each coal type which challenges the identification of a single capture criteria that would be applicable across different coal types.

Table 4.8. Simulation predictions of ash impaction rates on the ash probe surface (assuming 100% capture) and capture efficiency required to yield measured deposition rates

Case	Predicted ash impaction rate (g/m^2h)	Measured outside ash deposit growth rate (g/m^2h)	Required Capture Efficiency
PRB_AIR	2700	54 ± 1	2.3%
ILLINOIS_AIR	1400	124 ± 1	7.2%
SUFCO2_AIR	1100	339 ± 60	36%

Before testing a potential capture criteria method, one of the main motivations behind the work presented in this chapter was to study the sensitivity of simulation predictions of ash impaction rates to certain modeling parameters that are often overlooked in CFD ash deposition research. These two parameters are the resolution of the PSD model and the resolution of the mesh near the probe boundary. Table 4.9 presents the results of this sensitivity study. It is important to note that these impaction rates were calculated with a user-defined function for particle capture that is currently still in the early stages of development and did not yet have any capture/removal criteria defined, thus these rates still represent 100% capture. This difference in extraction methods explains the discrepancies between corresponding values in Tables 4.8 and 4.9 for the 40RR cases. In the PRB_AIR combustion model, the predicted impaction rate can vary by only about 12% depending on the resolution of the PSD model and the resolution of near-boundary mesh, while in the ILLINOIS_AIR and SUFCO2_AIR cases, predicted impaction rates can vary by 52% and 63% respectively with adjustments in these parameters. The number of bins in the PSD also

appeared to be less of an influential parameter in modeling ash particle behavior for the PRB coal, and much more significant for simulating the Illinois and Sufco 2 coal combustion ash particle behavior. This might be true because of the unique mineral matter compositions and physical structures of the ashes from different coals that are likely experiencing the effects of coagulation and fragmentation processes to different degrees. This emphasizes how challenging CFD modeling and simulation of ash deposition universally across fuel types can be. The results in Table 4.9 also indicate that further sensitivity testing is necessary to develop more confidence in a number of RR bins, and a spatial mesh resolution near the probe boundary that converge on more agreeable results for predicted ash impactions rates.

Table 4.9. Sensitivity of predicted ash impaction rates results to resolution of the Rosin-Rammler PSD model, and the use of a more refined spatial mesh resolution near the probe boundary

Case/Modeling Parameters			***Predicted ash impaction rates (g/m^2h)**
PRB_AIR	*coarse mesh*	*40RR*	1900
		80RR	1800
	fine mesh	*40RR*	2300
		80RR	2200
ILLINOIS_AIR	*coarse mesh*	*40RR*	4700
		80RR	1100
	fine mesh	*40RR*	3900
		80RR	2500
SUFCO2_AIR	*coarse mesh*	*40RR*	2100
		80RR	1100
	fine mesh	*40RR*	2600
		80RR	4600

* note that these values were obtained by a user defined function (assuming 100% capture) formulated to model particle capture/removal that is currently still in early development

4.4.3 Weber Number Capture Model Results

From the readily accessible particle data, individual particle Weber numbers can easily be calculated using the Weber number relationship in Equation 4.1. The average particle Weber number for each case can be seen in Table 4.10. The average particle Weber numbers from the three cases suggest that a simple Weber number capture criteria of 1 is not sufficient to adequately model ash deposition phenomena. A likely explanation is that surface

tension forces on a particle may be generally much larger than the particle's kinetic energy, which suggests that sticking forces are crucial to modeling capture tendencies. As a result, a more appropriate critical value of particle Weber number was identified in each case. These critical values are also listed in Table 4.10. When applied as capture criteria, meaning that any particle considered to have impacted the probe with a Weber number less than the critical value is further considered to actually capture/stick, capture efficiencies are achieved that when applied to predicted ash impaction rates, yield predicted ash deposition rates agreeable with experimental measurements. These results suggest that particle Weber number can be a suitable capture criteria, but for combustion in air, the critical Weber number appears to be unique to each coal type.

Table 4.10. Weber number capture criteria results from ash probe surface particle sample

Case	Average particle Weber number	Critical Weber Number	Predicted rate of ash deposition (g/m^2h)	Measured outside ash deposit growth rate (g/m^2h)
PRB_AIR	0.035	4.48E-05	56	54 ± 1
ILLINOIS_AIR	0.039	1.41E-04	120	124 ± 1
SUFCO2_AIR	0.041	1.96E-03	340	339 ± 60

Sensitivity of Weber number-based capture model was tested against the resolution of the particle size distribution model. Table 4.11 outlines the results. The calculated critical Weber number, due to its extremely small value, was found to differ significantly in some due to the sensitivity of the impaction rate results to the number of bins in the RR PSD

model. Additionally, in order to evaluate the robustness of using the critical Weber number as a capture criterion, the sensitivity of predicted ash deposition rates to the critical Weber number was explored to coal type was studied. Figure 4.12 illustrates this relationship. From these results it must be acknowledged that predicted ash deposition rates demonstrate moderate sensitivity to the critical Weber number. This is especially apparent in the PRB and Illinois coal cases near the identified appropriate cut off as a slight change (~10%) in the Weber cut off criteria can influence the predicted ash deposit growth rate by about 30%.

Table 4.11. The sensitivity of predicted ash deposition rates simulated using a critical Weber number capture criterion to the resolution of the parent fuel Rosin-Rammler PSD model

Case		Critical Weber Number	Predicted ash deposition rate (g/m^2h)	Measured outside ash deposit growth rate (g/m^2h)
PRB_AIR	**20RR**	3.85E-04	60.	54 ± 1
	40RR	2.19E-05	52	
	80RR	4.48E-05	56	
ILLINOIS_AIR	**20RR**	1.97E-04	130	124 ± 1
	40RR	2.34E-04	120	
	80RR	1.41E-04	120	
SUFCO2_AIR	**20RR**	2.25E-04	340	339 ± 60
	40RR	2.16E-03	340	
	80RR	1.96E-03	340	

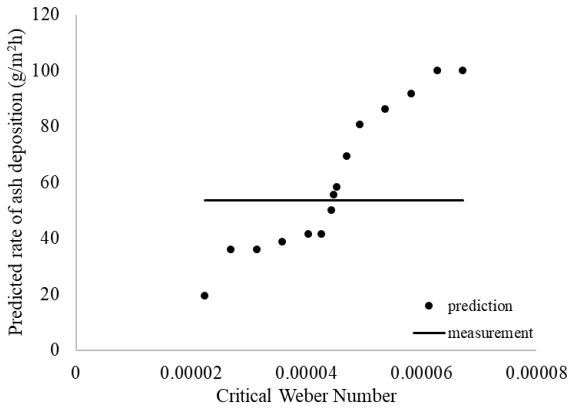

(a)

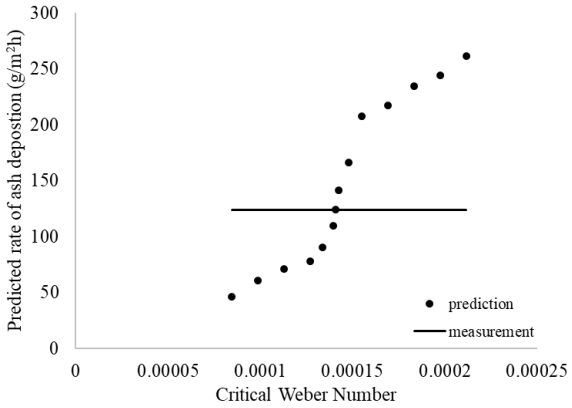

(b)

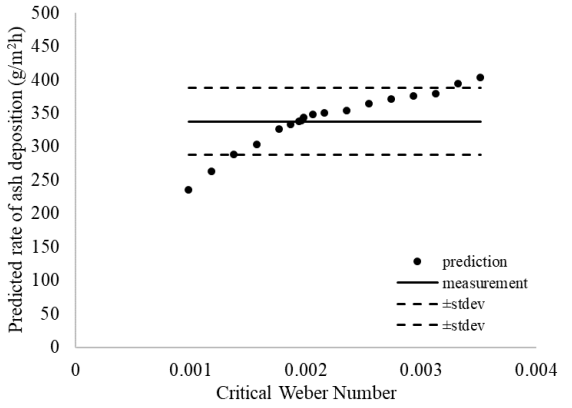

(c)

Figure 4.12. Sensitivity of predicted ash deposition rates to critical Weber number for cases: **a)** PRB_AIR **b)** ILLINOIS_AIR and **c)** SUFCO2_AIR

4.5 Conclusions

Ash formation and deposition is a complex physio-chemical process known to negatively affect boiler operation and involves several processes including vaporization, condensation, melting, nucleation, fragmentation, coagulation, impaction, and sticking propensity. Consequently, modeling these processes is quite challenging and requires the adequate characterization of multiple variables including the compositions of the coal and ash, physical properties of ash particles, and combustion conditions such as temperature and velocity fields. The research presented in this chapter focused on the following issues/challenges in modeling ash deposition resulting from coal combustion:

- Meeting/achieving spatial resolution requirements that are needed in the boundary layer adjacent to the deposition surface of interest in order to adequately characterize eddy impaction of particles
- Employing an adequate resolution (number of bins) to the initial distribution of particle sizes used in the simulation in order to more appropriately consider effects such as radiative heat transfer and ash formation represented by the evolution/shrinking of the particle sizes throughout the simulation
- Determine Weber number based capture criterion for multiple coal types by comparing simulation predictions for impaction rates to well characterized experimental measurements of ash deposit growth rates

These explorations were accomplished by simulating the combustion characteristics of three coals (PRB, Illinois and Sufco 2) in a 27kW down-fired combustor previously studied at the University of Utah. This configuration was chosen since well characterized experimental measurements of outer ash deposit growth rates were available and varied from 54 to 340 g/m^2h.

The temperature, velocity and outlet ash flux profiles were deemed to be adequately resolved since the coarse mesh (120K cells) and fine mesh (1,100K cells) simulations resulted in nearly identical predictions. However, significant variations in predicted ash impaction rates (that were estimated using add-on functions) were observed between the coarse and fine meshes across all three coal types. This is particularly noteworthy in light of the fact that the spatial mesh resolution near the probe in the fine mesh simulation was on the order of 10^{-4} m which is significantly more refined than the criterion required for ash deposition studies that has been proposed in literature. Additionally, a moderate sensitivity of the ash impaction rates to the number bins employed to resolve the coal PSD was also observed in both meshes. Again, it is worth mentioning that the number of "bins" employed to resolve the coal PSD (40-80 bins) far exceeds the 10 or 20 bins that are the norm in present-day combustion simulations.

Further, a Weber number based capture criterion was deduced to match the experimentally observed deposition rates. The Weber criterion varied significantly among the coals from $4.5x10^{-5}$ to $1.96x10^{-3}$ for the PRB and Sufco 2 coal cases respectively. The surprisingly small values suggested that sticking effects are perhaps more important to

modeling capture tendencies than inertial effects as previously thought. It was also demonstrated that a mere 10% adjustment to the critical Weber values can influence predicted deposition rates by up to 30%. This indicated that use of a universal capture criterion can lead to erroneous results.

REFERENCES (CHAPTER 4)

[1] Krishnamoorthy G, Wolf C. Assessing the Role of Particles in Radiative Heat Transfer during Oxy-Combustion of Coal and Biomass Blends. Journal of Combustion 2015;2015:1–15. https://doi.org/10.1155/2015/793683.

[2] Zhang J, Ito T, Ito S, Riechelmann D, Fujimori T. Numerical investigation of oxy-coal combustion in a large-scale furnace: Non-gray effect of gas and role of particle radiation. Fuel 2015;139:87–93. https://doi.org/10.1016/j.fuel.2014.08.020.

[3] Akar G, Sen S, Yilmaz H, Arslan V, Ipekoglu U. Characterization of ash deposits from the boiler of Yenikoy coal-fired power plant, Turkey. International Journal of Coal Geology 2013;105:85–90. https://doi.org/10.1016/j.coal.2012.12.001.

[4] Zhang J. OXY-COAL COMBUSTION: STABILITY OF COAXIAL PULVERIZED COAL FLAMES IN O2/CO2 ENVIRONMENTS. PhD Dissertation. University of Utah, 2010.

[5] Khatami R, Stivers C, Joshi K, Levendis YA, Sarofim AF. Combustion behavior of single particles from three different coal ranks and from sugar cane bagasse in O2/N2 and O2/CO2 atmospheres. Combustion and Flame 2012;159:1253–71. https://doi.org/10.1016/j.combustflame.2011.09.009.

[6] Zhan Z. ASH DEPOSITION AND ASH AEROSOL FORMATION MECHANISMS DURING OXY-COAL COMBUSTION. n.d.

[7] Nussbaumer T, International Energy Agency, Bioenergy Task 32: Biomass Combustion and Cofiring, Schweiz, Bundesamt für Energie, Kongress, editors. Aerosols from biomass combustion. Zürich: Verenum : Addresses for orders : Verenum; 2001.

[8] Syred N, Kurniawan K, Griffiths T, Gralton T, Ray R. Development of fragmentation models for solid fuel combustion and gasification as subroutines for inclusion in CFD codes. Fuel 2007;86:2221–31. https://doi.org/10.1016/j.fuel.2007.05.060.

[9] Seidel T, Krishnamoorthy G, Seames WS. Characterizing flame stability and radiative heat transfer in non-swirling oxy-coal flames using different multiphase modeling frameworks. Fuel 2019;256:115948. https://doi.org/10.1016/j.fuel.2019.115948.

[10] Seidel TL. Predicting Flame Stability, Ash Deposition And Radiative Heat Transfer Characteristics During Oxy-Fuel Combustion Of Pulverized Coal Using Different Multiphase Modeling Frameworks. University of North Dakota, 2019.

[11] ANSYS Fluent Theory Guide (19.1). ANSYS Inc. Online Manual Resource; Release 19.1.

[12] Rezaei D. CO-AXIAL TURBULENT DIFFUSION FLAMES WITH DIRECTED OXYGEN INJECTION. PhD Dissertation. University of Utah, 2013.

[13] Balachandar S, Eaton JK. Turbulent Dispersed Multiphase Flow. Annu Rev Fluid Mech 2010;42:111–33. https://doi.org/10.1146/annurev.fluid.010908.165243.

[14] Beckmann AM, Mancini M, Weber R, Seebold S, Müller M. Measurements and CFD modeling of a pulverized coal flame with emphasis on ash deposition. Fuel 2016;167:168–79. https://doi.org/10.1016/j.fuel.2015.11.043.

[15] Cai Y, Tay K, Zheng Z, Yang W, Wang H, Zeng G, et al. Modeling of ash formation and deposition processes in coal and biomass fired boilers: A comprehensive review. Applied Energy 2018;230:1447–544. https://doi.org/10.1016/j.apenergy.2018.08.084.

[16] Wang H, Harb JN. MODELING OF ASH DEPOSITION IN LARGE-SCALE COMBUSTION FACILITIES BURNING PULVERIZED COAL n.d.:16.

[17] Kleinhans U, Wieland C, Frandsen FJ, Spliethoff H. Ash formation and deposition in coal and biomass fired combustion systems: Progress and challenges in the field of ash particle sticking and rebound behavior. Progress in Energy and Combustion Science 2018;68:65–168. https://doi.org/10.1016/j.pecs.2018.02.001.

[18] Kleinhans U, Wieland C, Babat S, Spliethoff H. Large Eddy Simulation of a particle-laden flow around a cylinder: Importance of thermal boundary layer effects for slagging and fouling. Fuel 2019;241:585–606. https://doi.org/10.1016/j.fuel.2018.12.056.

[19] Weber R, Schaffel-Mancini N, Mancini M, Kupka T. Fly ash deposition modelling: Requirements for accurate predictions of particle impaction on tubes using RANS-based computational fluid dynamics. Fuel 2013;108:586–96. https://doi.org/10.1016/j.fuel.2012.11.006.

[20] Weber R, Mancini M, Schaffel-Mancini N, Kupka T. On predicting the ash behaviour using Computational Fluid Dynamics. Fuel Processing Technology 2013;105:113–28. https://doi.org/10.1016/j.fuproc.2011.09.008.

[21] Yong SZ. MULTIPHASE MODELS OF SLAG LAYER BUILT-UP IN SOLID FUEL GASIFICATION AND COMBUSTION. PhD Dissertation. Massachusetts Institute of Technology, 2010.

[22] Wang Y, Li X, Wendt JOL. On Ash Deposition Rates from Air and Oxy-Combustion of Pulverized Coal, Petroleum Coke, and Biomass. Energy Fuels 2019;33:5849–58. https://doi.org/10.1021/acs.energyfuels.8b04185.

[23] Chen L, Yong SZ, Ghoniem AF. Oxy-fuel combustion of pulverized coal: Characterization, fundamentals, stabilization and CFD modeling. Progress in Energy and Combustion Science 2012;38:156–214. https://doi.org/10.1016/j.pecs.2011.09.003.

[24] Borman GL, Ragland KW. Combustion Engineering. New York: McGraw-Hill Higher Education; 1998.

[25] Jones WP, Lindstedt RP. Global reaction schemes for hydrocarbon combustion. Combustion and Flame 1988;73:233–49. https://doi.org/10.1016/0010-2180(88)90021-1.

[26] Krishnamoorthy G. A new weighted-sum-of-gray-gases model for oxy-combustion scenarios: A new model for oxy-combustion scenarios. Int J Energy Res 2013;37:1752–63. https://doi.org/10.1002/er.2988.

CHAPTER 5

SUMMARY AND FUTURE WORK

5.1 Solids Dense Studies (Fluidized Bed and Granular Hopper)

An analogous collection of simulations of different conditions of both a fluidized bed and a hopper were developed in each of the three multiphase modeling frameworks available in MFiX. The three frameworks tested include the DEM, TFM, and MPIC models which differ in the degree of numerical resolution of representing solid-fluid interactions and solid-solid collision effects. Prediction results for the transient pressure profile in the fluidized bed simulations and the rate of mass discharge from the hopper simulations were analyzed to compare the capabilities and validity of physical predictions between the frameworks. An additional collection of simulations were carried out using the PETSc solver option for the pressure equation solver to assess the MFiX-PETSc integration across all three frameworks. The conclusions that can be drawn from the work presented in Chapter 3 can be summarized as follows:

- Simulations using the DEM framework produced the most accurate predictions compared to experimental measurements for physical flow attributes in the fluidized bed study. DEM predictions for time averaged pressure drop in the fluidized bed study agreed with

experimental measurements within 10% using the native pressure solver option. Using the PETSc solver, prediction accuracies were decreased in the DEM framework despite the overall computational advantage observed when using the PETSc solver.

- The DEM simulations required the most computational effort of all three frameworks, with a substantial portion attributed to resolving particle collisions. A reduction in computational effort was achieved by using the PETSc pressure solver in the DEM framework by roughly 4-20%. However as mentioned above, the PETSc solver did decrease the fidelity of the DEM predictions.

- The PETSc solver proved to be more robust than the native pressure solver in all three frameworks by requiring a lower number of outer iterations resulting in the ability to use larger time steps. This improvement was more significant in the DEM framework and is likely the source of the improvement in overall computational cost observed when using the PETSc solver in the DEM framework, and is also likely the fault of the decrease in accuracy observed.

- The TFM framework was able to produce simulation predictions for physical flow characteristics that agreed quite well with the DEM framework in both the fluidized bed and hopper studies while requiring just over half of the amount of computational effort in terms of CPU hours. TFM predictions for average pressure drop in the fluidized bed study were within 36%, and when using the PETSc solver this level of accuracy was maintained but mildly increased the solve time. In the hopper study, pure granular flow

simulations in the TFM framework produced almost identical discharge rates to those of the DEM framework which were considered to be the benchmark gold standard in the hopper study. However the TFM simulations proved to encounter great difficulties converging solutions for solids pressure in 3D pure granular flow.

- The MPIC framework resulted in the fastest solve times in both studies by roughly 93% on average, and demonstrated to be strongly influenced by the computational bottleneck associated with solving the pressure equations like observed in previous work on TFM simulations. Unfortunately, the MPIC framework failed to give reasonably valid predictions of physical flow behaviors compared to those predicted by the much more highly resolved DEM framework. In the fluidized bed study, the MPIC framework predictions for transient pressure profiles were not very realistic and compared poorly to experimental measurements. In the hopper study, the MPIC framework predicted emptying times almost 2-3 times longer than the other two frameworks. This highlights the restrictions of the MPIC framework to more dilute flows, and emphasizes the importance of more rigorous development of the empirical MPIC solids stresses models especially in flow regimes with higher solids densities.

In future work stemming from the research presented in Chapter 3 of this thesis, further investigation in 3D of fluidized bed flows in the DEM framework using the PETSc solver is warranted. Additionally, another natural extension of this work would be to translate the hopper models that were developed in the present work into the MFiX-PETSc integration

version. This would allow more testing, particularly in the TFM framework, of the PETSc solver performance in pure granular flows in terms of ease of convergence and speed.

5.2 Dilute Dispersed Solids Studies (Ash Deposition)

In this chapter, CFD models in ANSYS Fluent's DPM framework were developed and simulations carried out of three select experimental cases in a coal with air fired combustor at the University of Utah. The three coal types of interest were: PRB (sub-bituminous), Illinois (bituminous), and Sufco 2 (Utah-bituminous), with distinctly different measured outer ash deposit growth rates ranging from 54 to 340 g/m^2h. The purpose of these models was in the aim of developing an ash particle capture/removal sub model based on Weber number criteria to deduce capture efficiencies to be imposed on simulation predictions for impaction rates that can predict accurate ash deposition rates. Unfortunately, current state-of-the-art Lagrangian tracking methods for modeling a combusting particle use a simple "shrinking core" model formulation to alter the PSD of the combusting particle since incorporating additional physio-chemical processes such as fragmentation, nucleation, coagulation and condensation to alter the PSD are very difficult. Thus, the main focus of this research was to assess the sensitivity of simulation predictions for ash impaction rates to the resolution of the PSD model and to the spatial resolution in the boundary layer. The resolutions employed in this work exceeded limits/expectations commonly proposed in literature (at least 40 RR bins and at least 10^{-4} m near-boundary spatial resolution). Results from this work demonstrate the challenges often encountered in modeling the ash deposition

process as it is still not fully understood, and highlights the need for more collaborative efforts between CFD modelers and experimentalists.

- Predicted temperature and velocity profiles at different axial distances from the burner, and flue gas ash concentrations were in good agreement with the measurements/estimates across all 3 coal types, indicating the adoption of appropriate combustion modeling methodologies.
- Sensitivity of the temperature and velocity predictions to different mesh resolutions and the number of bins employed to resolve the coal PSD was also assessed. The profiles were only marginally impacted, specifically near the location of the collector probe, by these variations in modeling parameters.
- Absolute rates of particle impaction/deposition assuming 100% capture were found to be much greater than the measured values ranging from 2700 to 1100 g/m^2h in the PRB and Sufco 2 cases respectively. This result indicated that attempting to model ash particle impaction alone is not enough to accurately predict deposit growth rates and enforces the importance of capture efficiency and formulating a particle capture sub model. Corresponding capture efficiencies were calculated in each case and ranged from 2% in the PRB case, to 36% in the Sufco 2 case.
- Ash impaction rates proved to be sensitive to the number of bins used to resolve the PSD, but the degree of this sensitivity was unique to each coal type. The PRB coal cases seemed to be the least influenced by the bin resolution, while the Illinois and Sufco 2 coal

type cases produced simulation predictions for ash impaction rates that increased by almost half when doubling the number of bins from 40 to 80.

- Near-boundary mesh sensitivity study results for ash impaction rates were significantly influenced by the spatial resolution near the probe surface which pointed to a need to adequately resolve the boundary layer in order to better predict particle impaction and capture behavior in future modeling efforts.
- Based on the coarse mesh and 40RR simulation results, appropriate capture efficiencies and critical Weber numbers were identified for each coal type. The Weber cutoff values were well less than 1 and varied significantly between the coal types, pointing to the importance of appropriately considering attraction forces which are influenced by the coal compositions.
- Predicted deposition rates employing the Weber number based capture method using the critical values identified as capture criteria agreed well with measured values, but demonstrated sensitivity to the number of PSD model bins. In the PRB and Illinois coal cases, a mere 10% adjustment in the critical Weber cutoff value showed to change predicted deposition rates by roughly 30%, demonstrating that the critical Weber number approach to modeling particle capture is not universal and should be used with caution.

In future work following the insights gained from these studies, further developments and improvements to the particle capture/removal model need to be made including identifying and testing other capture formulations. Attention should be given to sticking

effects and surface tension relationships in determining particle capture as opposed to primarily momentous effects. Additionally, more modeling parameter sensitivity studies should be conducted to improve upon the models developed in this work, and to extend the efforts into the realm of oxy combustion, and in the realm of biomass and coal/biomass blended fuels.